KTH ROYAL INSTITUTE
OF TECHNOLOGY

Degree Project in Electric Power Engineering

Second cycle, 30 credits

Reliability and Cost-Benefit Analysis of the Battery Energy Storage System

DITA ANGGRAINI

Stockholm, Sweden, 2023

Reliability and Cost-Benefit Analysis of the Battery Energy Storage System

DITA ANGGRAINI

Master's Programme, Electric Power Engineering, 120 credits
Date: June 30, 2023

Supervisors: Zhongtian Li, Jaime Garcia
Examiner: Patrik Hilber
School of Electrical Engineering and Computer Science
Host company: Northvolt Systems AB
Swedish title: Tillförlitlighet och Kostnadsnyttoanalys av Batterienergilagringssystemet

Abstract

The battery energy storage system (BESS) is crucial for the energy transition and decarbonisation of the energy sector. However, reliability assessment and capital cost challenges can hinder their widespread deployment. Reliability and cost-benefit analysis help address these challenges and assess BESS adoption's feasibility and viability, which is the aim of this project.

A BESS contains various components such as battery packs, inverters, a DC/DC converter, a Battery Thermal Management System (BTMS), electrical protection devices, a transformer, and an Energy Management System (EMS). All these fundamental components must be considered to obtain a complete reliability prediction. Most previous studies focused on the reliability analysis of individual components, but few consider all the abovementioned components in collective reliability analysis. In this thesis, each component is mathematically modelled to estimate failure rates and then used to predict the reliability of the overall BESS system. The model accuracy is verified by comparing the computed reliability indices with the values from standards/references, showing that the proposed reliability prediction methods provide reasonable outcomes.

Different scenarios to enhance BESS reliability through component redundancy are explored in this project. It is proved that applying component redundancy can boost the overall BESS reliability at the price of an increased capital cost. However, the enhancement in reliability and lifespan due to component redundancy can also curtail maintenance costs. A cost-benefit analysis assesses each scenario's profitability, considering manufacturers' and owners' perspectives. It helps determine the optimal balance between reliability and profitability. Redundancy applied to components with higher failure rates and lower costs improves the reliability and profitability of the BESS. The finding highlights the importance of strategic component selection for enhancing BESS reliability. Careful reliability and cost analysis should be performed simultaneously to find the most optimised BESS scenario.

Keywords

Battery Energy Storage System, Cost-Benefit Analysis, Prediction Methods, Reliability Analysis

Sammanfattning

Batterienergilagringssystemet (BESS) är avgörande för energiomställningen och avkarboniseringen av energisektorn. Tillförlitlighetsbedömning och utmaningar med kapitalkostnader kan dock hindra deras utbredda användning. Tillförlitlighet och kostnads-nyttoanalys hjälper till att hantera dessa utmaningar och utvärdera BESS-antagandets genomförbarhet och genomförbarhet, vilket är syftet med detta projekt.

Ett BESS innehåller olika komponenter som batteripaket, växelriktare, en DC/DC-omvandlare, ett Battery Thermal Management System (BTMS), elektriska skyddsanordningar, en transformator och ett energiledningssystem (EMS). Alla dessa grundläggande komponenter måste beaktas för att få en fullständig tillförlitlighetsförutsägelse. De flesta tidigare studier fokuserade på tillförlitlighetsanalys av enskilda komponenter, men få beaktar alla ovan nämnda komponenter i kollektiv tillförlitlighetsanalys. I denna avhandling modelleras varje komponent matematiskt för att uppskatta felfrekvensen och används sedan för att förutsäga tillförlitligheten hos det övergripande BESS-systemet. Modellens noggrannhet verifieras genom att jämföra de beräknade tillförlitlighetsindexen med värdena från standarder/referenser, vilket visar att de föreslagna metoderna för tillförlitlighetsprediktion ger rimliga resultat.

Olika scenarier för att förbättra BESS-tillförlitligheten genom komponentredundans utforskas i detta projekt. Det är bevisat att tillämpning av komponentredundans kan öka den övergripande BESS-tillförlitligheten till priset av en ökad kapitalkostnad. Förbättringen av tillförlitlighet och livslängd på grund av komponentredundans kan dock också minska underhållskostnaderna. En kostnads-nyttoanalys bedömer varje scenarios lönsamhet, med hänsyn till tillverkarnas och ägarnas perspektiv. Det hjälper till att bestämma den optimala balansen mellan tillförlitlighet och lönsamhet. Redundans som tillämpas på komponenter med högre felfrekvens och lägre kostnader förbättrar tillförlitligheten och lönsamheten för BESS. Resultatet belyser vikten av strategiskt komponentval för att förbättra BESS-tillförlitligheten. Noggrann tillförlitlighets- och kostnadsanalys bör utföras samtidigt för att hitta det mest optimerade BESS-scenariot.

Nyckelord

Batterienergilagringssystem, Förutsägelsemetoder, Kostnads-nyttoanalys, Tillförlitlighetsanalys

Acknowledgments

I want to express my deepest gratitude to all those who have supported and contributed to completing this master's thesis. First and foremost, I extend my heartfelt appreciation to my supervisors, Zhongtian Li and Jaime Garcia. Despite their busy schedules, they have consistently provided me with guidance and support throughout this journey. I am also sincerely grateful to my examiner, Patrik Hilber, for his feedback, advice, and insights that enrich my project. Their mentorships and guidance have been instrumental in shaping my research direction and the execution of this project.

I want to thank the Northvolt team, who have supported me throughout my master's thesis project. Their knowledge and expertise in Battery Energy Storage Systems (BESS) have been invaluable, and I am grateful for the opportunity to work with such an exceptional team.

Thank you to the Electric Power Engineering department faculty member for their teachings and learning support. Their expertise and knowledge have been influential and inspiring toward my academic journey.

Furthermore, I would like to acknowledge the countless researchers and scholars whose groundbreaking academic results have become the foundation of my research.

Finally, I am forever indebted to my family and friends for their unwavering support and encouragement throughout this thesis project. Their belief in me always motivates me, and I am grateful for their presence. Once again, thank you so much to all those who participated in this thesis completion.

Stockholm, June 2023
DITA ANGGRAINI

Contents

List of Figures

List of Tables

List of acronyms and abbreviations

3L-NPC	Three-Level Neutral Point Clamped
AC	Alternating Current
BESS	Battery Energy Storage System
BMS	Battery Management System
BOP	Balance of Power
BTMS	Battery Thermal Management System
cdf	Cumulative Distribution Function
CMM	Capability Maturity Model
CND	Can Not Duplicate
DC	Direct Current
DCPM	Direct Current Protection Module
DOD	Depth of Discharge
DSL	Defect Stabilisation Level
EMS	Energy Management System
EOL	End of Life
ESS	Energy Storage System
FD	Fault Density
FPMH	Failures per million hours
HST	Hottest-Spot Temperature
HVAC	Heating, Ventilation, and Air Conditioning
IEEE	Institute of Electrical and Electronics Engineers
IGBT	Insulated-Gate Bipolar Transistor
IMD	Insulation Monitoring Device
LCC	Life Cycle Cost
Li-Ion	Lithium-Ion
MCCB	Molded Case Circuit Breaker

MSS	Multi-State System
MTBF	Mean Operating Time Between Failure
MTTF	Mean Time To Failure
Na-S	Sodium-Sulfur
Ni-Cd	Nickel-Cadmium
Ni-MH	Nickel-Metal Hydride
NPF	Net Present Factor
NPS	Net Present Sum
NPV	Net Present Value
OIP	Oil Impregnated Paper
PbA	Lead-acid
PCB	Printed Circuit Board
PCM	Phase Change Materials
PCS	Power Conversion System
pdf	Probability Distribution Function
PGF	Process Grading Factors
RBESS	Reconfigurable Battery Energy Storage System
RFB	Redox Flow Battery
RIAC	Reliability Information Analysis Center
SDG	Sustainable Development Goal
SEI	Software Engineering Institute
SMC	Surface Mounted Component
SOH	State of Health
TCC	Total Capital Cost
TEAM	Thermal, Electrical, Ambient and Mechanical
UGF	Universal Generating Function
UN	United Nations

List of Symbols Used

The following symbols will be later used within the body of the thesis.

α Threshold value of SOH before End of Life [in decimal form]

$\cos(\varphi)$ Power factor [in decimal form]

ΔQ_{fade} Battery capacity loss [in decimal form]

γ Shape parameter for the Weibull distribution

λ Failure rate [failure per million hours or failure] or [f/yr]

λ_{EB} Environmental base failure rate

λ_{EOS} Failure rate multiplier, solder joint delta temperature

λ_{fbx} Failure rate of through holes [failure per million hours]

λ_{OB} Base failure rate in operating condition

λ_{sbx} Failure rate of SMC [failure per million hours]

λ_{SJB} Solder joint base failure rate

λ_{TCB} Base failure rate, temperature cycling

π_C Capacitance failure rate multiplier

π_G Reliability growth failure rate multiplier

Π_P Parts process factor

π_P Failure rate multiplier for resistor

π_S Failure rate multiplier, stress

π_{cbx} Influence factor for the number of layers for PCB failure rate

π_{CR} Failure rate multiplier, cycling rate

π_{DCN} Failure rate multiplier, duty cycle, non-operating

π_{DCO} Failure rate multiplier for duty cycle

π_{DT} Failure rate multiplier, delta temperature

Π_D The design process factor

Π_E The environmental factor

Π_G The reliability growth factor

Π_{IM} The infant mortality factor

Π_I The induced process factor

π_{Lbx} PCB's track width's coefficient

Π_M The manufacturing process factor

Π_N The no-defect process factor

π_{RHT} Failure rate multiplier for temperature-humidity

π_{SJDT} Failure rate multiplier for solder joint delta temperature

Π_S The system Management process factor

π_{tbx} Temperature influence factor for PCB failure rate

π_{TE} Failure rate multiplier, temperature – environment

π_{TO} Failure rate multiplier for temperature during operating condition

Π_W The wear out process factor

θ Scale parameter for the Weibull distribution

$_D$ Subscript for diode

$_I$ Subscript for IGBT

$_i$ Subscript representing item i

$_P$ Subscript for a predicted value

$_{s}$ Subscript representing system

$_{T}$ Subscript for transformer

$_{t}$ Subscript for time

$_{BTMS}$ Subscript for battery thermal management system

$_{con}$ Subscript for conduction loss

$_{DCDC}$ Subscript for DC/DC converter

$_{DCPM}$ Subscript for DC Protection Module

$_{electromech}$ Subscript for electromagnetic devices

$_{EMS}$ Subscript for Energy Management System

$_{IA}$ Subscript for initial assessment value

$_{INV-S}$ Subscript for inverter system

$_{INV}$ Subscript for inverter

$_{PCB}$ Subscript for printed circuit board

$_{ref}$ Subscript for reference current/voltage (semiconductor)

$_{SMC}$ Subscript for surface mounted components in PCB

$_{swi}$ Subscript for switching loss

$_{SW}$ Subscript for software

Ah Total ampere-hour throughput of battery [Ah]

AS Software's average severity, fraction of disruptive faults [in decimal form]

B Pre-exponential factor

B_{10} B10 value

C Capacitance [microfarads]

C_B Battery cell's/module's/ pack's capacity under a specific operating condition [Ah]

C_{cap} Total capital cost per unit power [€/kWh]

CR Cycling rate: the power cycle number per year to which the system is exposed [cycles/yr]

DC Duty cycle, fraction of the calendar time when a system is in operation [in decimal form]

$DC_{1op/1nonop}$ Constant that is applied to a specific electronics item from RIAC 217 plus™

DSL Software's defect stabilisation level

$E_{on/off}$ IGBT's energy losses during on/off state [J]

Ea_{op} Activation energy [J/mol]

$F(t)$ Cumulative distribution function

$f(t)$ Probability distribution function

F_0 Software's initial defect density

f_{swi} Switching frequency [Hz]

F_{t-i} The number of software faults remaining at time ti [failures]

FA Software's fault activation, the fraction of population exhibits fault activation [in decimal form]

FL Software's fault latency

g_l Battery SOH level in the UGF function [in decimal form]

I_B Battery charge/discharge current [A]

$KSLOC$ Software's source codes' lines, excluding comments [in thousands]

m Semiconductor's modulation index

N Number of an item connected in a system [units]

N_c Total number of cycles before battery end of life [cycles]

N_f Number of lines that connect every hole in PCB

n_i Number of item$-i$

N_s Number of lines that connect each PCB component

N_{pbx} The number of tracks in PCB

N_{tbx} The total number of holes in PCB

OC Operating cycles per hour for electromagnetic device [cycles/hr]

P Resistor-rated power [W]

p The probability of an item/system failure [in decimal form]

P_B Battery cell's/module's/ pack's power [kW]

P_i Power loss of item$-i$ [W]

Q_B Battery cell's/module's/ pack's nominal capacity [kWh]

q_l Probability that the battery SOH falls in the level in g_l [in decimal form]

$Q_{current}$ Maximum charge capacity of the aged battery cell/module/pack [kWh]

Q_{fade} Capacity fade or loss of the battery cell/module/pack [kWh]

Q_{ini} Maximum charge capacity of the new battery cell/module/pack [kWh]

R Ideal gas constant (8.31 J/mol K)

r Interest rate [in decimal form]

$R(t)$ Reliability or survivor function

$R_i(t)$ Reliability of item i at time$-t$ [in decimal form]

$r_{CE/T}$ IGBT's/diode's resistance [Ω]

R_{CH} Thermal resistances from heat sink to ambient temperature [K/W]

R_{TH} Thermal resistances from the junction to interface case of a semiconductor device [K/W]

RH Relative humidity [in decimal form]

RV Residual value [€]

T Temperature [°C]

t_p	The p-level quantile
T_R	Actual temperature rise [°C]
t_s	Software's time to stabilisation
T_{AE}	Ambient temperature during non-operational state [°C]
T_{AO}	Ambient temperature during operational state [°C]
T_{vj}	Junction temperature on heat sink [°C]
U_{CE0}	IGBT's voltage drop [V]
U_{d0}	Diode's voltage drop [V]
U_{DC}	DC voltage at DC side [V]
U_l	Line-to-line voltage [V]
U_{RMS}	RMS voltage or AC terminal voltage [V]
Y	Manufacture year of a component
y	Technical lifetime of the system [yr]
z	Power law factor
$z(t)$	Failure or hazard rate

Chapter 1

Introduction

1.1 Background

To achieve the Paris Agreement objectives, global renewable energy must be escalated to at least six times faster than the current global strategies. Over the past few years, energy intensity has consistently fallen around 1.8% annually. To achieve more significant progress, the fall rate has to accelerate by one-and-a-half times to 2.8% per year. The renewable energy proportion in total final energy consumption has to be increased from 18% in 2015 to 65% in 2050. A decarbonised power sector, dominated by renewable energy, is the core of the energy transition [1]. On accelerating the penetration of renewable energy sources and accommodating their intermittent nature, there is a challenge to maintain secure and reliable operation of the power grid [2][3]. Battery Energy Storage System (BESS) provides an effective solution to support the balancing between electricity supply and demand with the integration of renewable energy generation to the grid if the BESS can be made cost-effective [4].

While stationary BESS has been used in many sectors, a radical solution of a more mobile and transportable BESS can provide greater flexibility of decarbonised energy source relocation and redeployment at different sites [5]. A mobile BESS can replace diesel generators with renewable alternatives and alleviate the territorial limitation of providing decarbonised energy [5]. Even though the focus of the study is based on the mobile BESS, in the electrical system perspective, it is the same with a stationary BESS, therefore in the following discussion, BESS is used as the primary terminology.

BESS can be used for peak shaving, eliminating consumption spikes and reducing the operation cost in consumer sites. Uncertainty of the system reliability is a primary obstacle in the BESS design. How to assess the

reliability of the BESS and its subsystems is a focal issue [6][7]. A prediction for Mean Time To Failure (MTTF) is desirable before a new product is ramped up to sell to customers [8]. Furthermore, it is essential to understand the economic aspect of BESS for development and deployment. The lack of adequate information and tools to analyse the cost of BESS can hinder the establishment of feasible business models, regulation strategies, and ownership structure [9].

1.2 Problem

1.2.1 Original Problem and Definition

A BESS contains numerous Alternating Current (AC) and Direct Current (DC) components which influence the overall system's reliability. The operating and environmental conditions, such as temperature, humidity, load current, etc., can affect the reliability of the BESS. It is essential to predict the reliability of overall BESS from the design phase and investigate how to improve it. In addition to the technical side, a feasible business model is necessary to enable BESS adoption. The trade-off between reliability and profitability must be carefully considered in the BESS design.

1.2.2 Research Question

The thesis project mainly wants to answer the following questions:

- How to develop a method to predict the overall reliability of the BESS?
- How to perform BESS cost-benefit analysis to strike an optimum trade-off between BESS reliability and profitability?

1.3 Purpose

The main objective of this thesis project is to develop a method to estimate the overall reliability and cost of the BESS in the design phase. The reliability prediction method can be used to assess the BESS reliability at the component or system level, which can be helpful as an input to improve the system's design. Analysing cost-benefit can also provide additional insight into the economic feasibility of a particular BESS design. Therefore, a balanced trade-off between reliability and profitability of the BESS can be achieved.

If the project's objective is achieved, Northvolt System AB, as the host company, can use the outputs of this project in their analysis or design process. The reliability analysis methods can be helpful as a summary for other parties who want to conduct similar calculations. It is important to note that the data published in this project is public data/ published literature.

1.4 Research Methodology

A mix of qualitative and quantitative analyses is performed in this project. Qualitative analysis is essential when identifying different fault modes of the system. At the same time, the quantitative analysis provides a more significant portion of estimating the reliability indices of each component. A probabilistic distribution method is utilised in the reliability prediction.

The cost-benefit analysis uses cost data from published literature to determine each subsystem's average cost. Total Capital Cost (TCC) and Life Cycle Cost (LCC) analyses are computed to evaluate the BESS's cost. It is interesting to study the economic perspective of the manufacturer and owner of the BESS. Net Present Value (NPV) method is selected on the LCC analysis to analyse the cost during the entire system's lifetime. Available data from the literature/standards are utilised for the computations. The results are validated by checking the consistency with available resources.

Figure 1.1 visualises the methodology of the research.

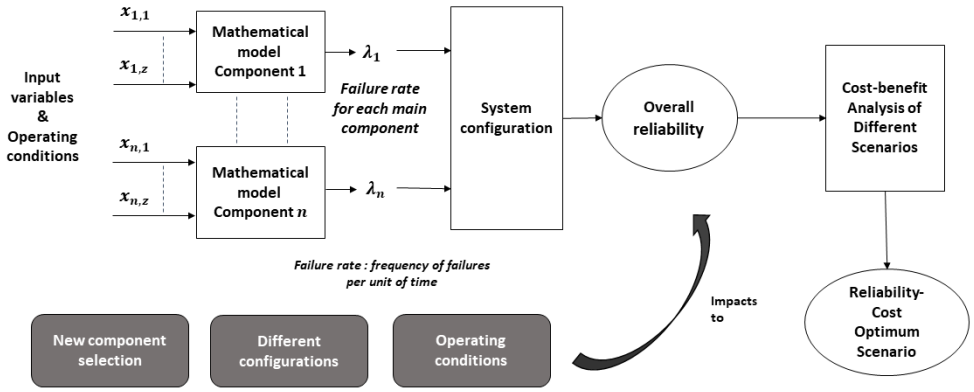

Figure 1.1: Research process

The steps in the process are detailed below:

Step 1 Literature review,

Step 2 Build the mathematical models of each subsystem,

Step 3 Relevant data collection,

Step 4 Calculate the individual component's failure rate,

Step 5 Define the configuration of the analysed system,

Step 6 Calculate the overall reliability of the BESS,

Step 7 Perform cost-benefit analysis of different BESS scenarios,

Step 8 Validity and sensitivity analysis,

Step 9 Report writing.

1.5 Delimitations

The delimitations of this thesis project are listed below:

- The Battery Thermal Management System (BTMS) and Battery Management System (BMS) reliability indices are cited from other research, but the computation methodology is given to reproduce the results.
- Only fundamental components included in the reliability analysis are considered in the cost-benefit analysis.
- The ageing mechanisms of the battery cells during charge and discharge is assumed to be the same.
- Calendar ageing of the battery cells is neglected.
- Cost of each sub-component is approximated from the available literature or market price.
- In the case of parameter values lacking literature resources, they are assumed using reasonable values based on average market prices.

1.6 Structure of the Thesis

Chapter 1 provides the introduction of the research. Chapter 2 presents relevant theoretical background information about BESS components. Chapter 3 presents the methodology and method used to predict the reliability of each component and overall BESS. Chapter 4 presents the methods used for the

cost-benefit analysis of different BESS scenarios from the manufacturer and ownership perspective. Chapter 5 presents the results and discussion from the reliability computation based on the calculation methods. Chapter 6 discusses the trade-off between reliability and profitability of different BESS scenarios. Chapter 7 provides the conclusion and future work recommendations.

Chapter 2

BESS Theoretical Background

2.1 Battery Energy Storage System

Having several advantages such as rapid power response, high energy density, and flexible deployment; BESS serves a vital role in various applications from frequency regulation, peak shaving, balancing of renewable energy fluctuation to economic dispatch [6][10][11]. Studying and improving BESS reliability for development and deployment is crucial. Overall, the reliability of the BESS depends on its battery power, system topology, control system, and management techniques [2].

While many other factors significantly affect the viability of the BESS, the cost has one of the most significant impacts. Over the past few years, there has been a substantial reduction of the BESS cost; however, it is vital to conduct a cost-benefit analysis and study BESS profitability. The life span of an energy storage device is an essential factor in reviewing its economic efficiency [12]. Reliability and cost of BESS impact each other, and it is interesting to study their relationship.

A BESS mainly consists of Energy Management System (EMS), battery system, BTMS, and power conversion system. In connection with the grid in a different voltage level, the BESS is connected through a transformer [12]. In addition, there are several electrical protection devices needed to protect the BESS when failures happen, such as the Molded Case Circuit Breaker (MCCB) and Direct Current Protection Module (DCPM). The individual component theoretical background is provided in the following sections.

2.1.1 Li-Ion Battery Packs

There are various chemistry types of battery, such as Lead-acid (PbA), Nickel-Cadmium (Ni-Cd), Nickel-Metal Hydride (Ni-MH), Lithium-Ion (Li-Ion), Sodium-Sulfur (Na-S), and Redox Flow Battery (RFB). The Li-Ion batteries are considered safe and have the highest energy density [12]. The specific energy of Li-Ion battery varies from $100 - 265$ Wh/kg [13][14], while the volume energy density varies from $177 - 677$ Wh/L, and efficiency reaches $92 - 95\%$. The lifetime differs from $500 - 20\ 000$ cycle, or $5 - 20$ years [14][15]. In addition, Li-Ion battery has a mature packaging, fast response (in milliseconds), and low discharge rate [14]. The drawbacks of Li-Ion batteries are substantial upfront expenses, potential safety concerns, and rapid degradation if experiencing frequent deep charging and discharging, leading to reduced power capacity over time [14][16]. Due to its various advantages above, in this project, Li-Ion battery is selected in the case study. Failure modes of Li-Ion battery are summarised in Table 2.1.

2.1.2 Power Converter System

Field experiences conducted in [18][19] show that power electronics converters are a weak link with considerable impacts on the overall reliability of electrical systems [20]. There are two types of power converters in BESS, AC/DC (inverter) and DC/DC converter. They mainly consist of semiconductors devices, such as Insulated-Gate Bipolar Transistors (IGBTs), diodes, and capacitors.

Industry-based survey [21] shows that semiconductor switches and capacitors are the most vulnerable components in power converters. The system's transient and unexpected overloads are the primary cause of random failures, while thermal stresses, mechanical vibrations, and humidity are the main reasons for long-term wear-out failures.

2.1.2.1 Inverter System

A bidirectional inverter converts power from AC line voltage and DC battery terminals and authorises the power flow both ways during the charge and discharge process [22]. It mainly consists of semiconductor modules (IGBTs, diodes, and capacitors). The lifespan of power electronics components is drastically reduced due to high temperature; therefore, cooling fans are usually used to generate airflow to cool the electronics components [23]. Failure rates of semiconductor devices depend on the power losses, which are directly

Component	Failure Mode	Consequences
Anode	Solid electrolyte interphase layer thickening, particle fracture, decreased electrode porosity, Lithium plating, dendrite growth, free copper particles or plating	Increased resistance of charge transfer, capacity reduction, power reduction, increased diffusion resistance, short circuit
Cathode	Solid electrolyte interphase layer thickening, particle fracture, electrode porosity reduction, gas production, cell casing's bloating, pitting aluminium corrosion	Increased resistance of charge transfer, capacity reduction, power reduction, increased resistance, increased diffusion resistance, current density reduction
Separator	Hole in the separator and closing of the separator poles	Production of high heat, cell casing's bloating, extreme voltage decrease
Li-Ion	Li-Ion reduction, layer thickening of solid electrolyte interphase	Capacity reduction
Organic solvent	Cell casing bloating, gas generation, layer thickening of solid electrolyte interphase	Increased diffusion resistance, thermal runaway, transfer resistance charge increase, capacity and power reduction
Terminals	External corrosive path, cracking of solder joint	Generation of high heat, cell casing bloating, extreme voltage drop, loss conductivity between the host device and battery
Casing	Short circuit between cathode and anode	High heat production, bloating of cell casing, extreme voltage drop

Table 2.1: Li-Ion battery failure modes [17]

affected by the level of currents flowing. It means that the reliability of an inverter depends on the C-rate and the operating temperature [2].

There are various types of bidirectional inverters. The Three-Level Neutral Point Clamped (3L-NPC) inverter has become an attractive solution among different topologies of multilevel inverters. 3L-NPC inverter has high efficiency, good capability of losses distribution, lower power losses, and smaller current ripple output [24][25]. However, it has the disadvantage of higher complexity making the circuit significantly sensitive toward parasitic effects, which can increase the switch-off losses of the transistors. This loss can be minimised by carefully designing the module pinning [25].

There are two types of inverter failure categories: over-stress and wear-out. The over-stress failure can be caused by over voltage, over current, Thermal, Electrical, Ambient and Mechanical (TEAM) stress, thermal runaway, or flashovers. The wear-out failure category can be caused due to time-dependent

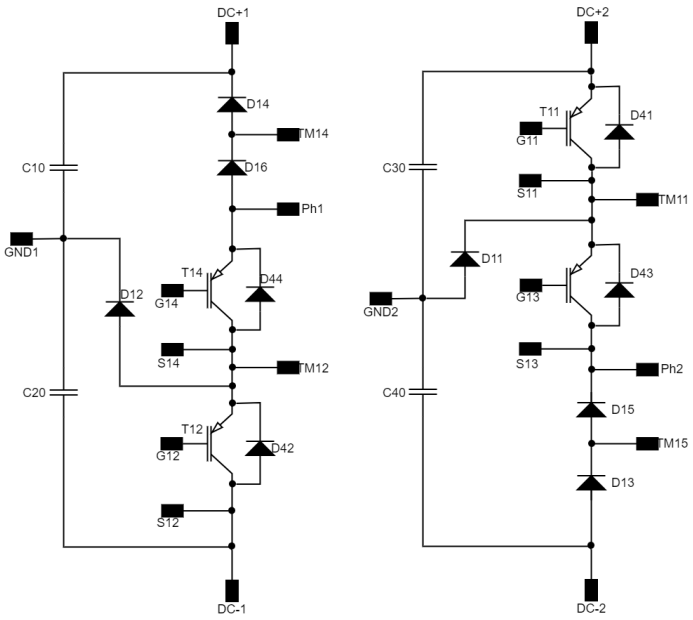

Figure 2.1: IGBT module on the inverter [26]

dielectric breakdown, insulation degradation, thermo-mechanical fatigue, electrochemical migration, or hot carrier injection [27][28][29][30][31].

High ambient temperature significantly affects power electronics items' service life inside an inverter. Therefore, A cooling system is necessary to stop overheating power electronics components. There are two types of power electronics cooling in the market: passive and active. *Passive cooling* leans on natural convection; heat sinks can be used to keep the temperature below a certain level. While in *active cooling*, proactive interior fans are used to eliminate warm air in a controllable manner to avoid overheating. In addition to the heat sink, one or more fans can circulate the air inside the inverters and avoid hot spots [32].

The IGBT module used on the inverter in this study is shown in Figure 2.1. The life expectancy of the module can vary; usually, it can range between 20 to 40 years, determined by the operational conditions of the module [27][33].

2.1.2.2 DC/DC Converter

DC/DC converter is a system consisting of energy-storing elements, high-frequency switches, and filtering elements [34]. It is used to generate regulated high power efficiency DC output voltage from a DC input source [34][35].

DC/DC converter controls the DC flow between the battery packs to the low voltage electronics components in the BESS. A schematic of DC/DC converter module is given in Figure 2.2.

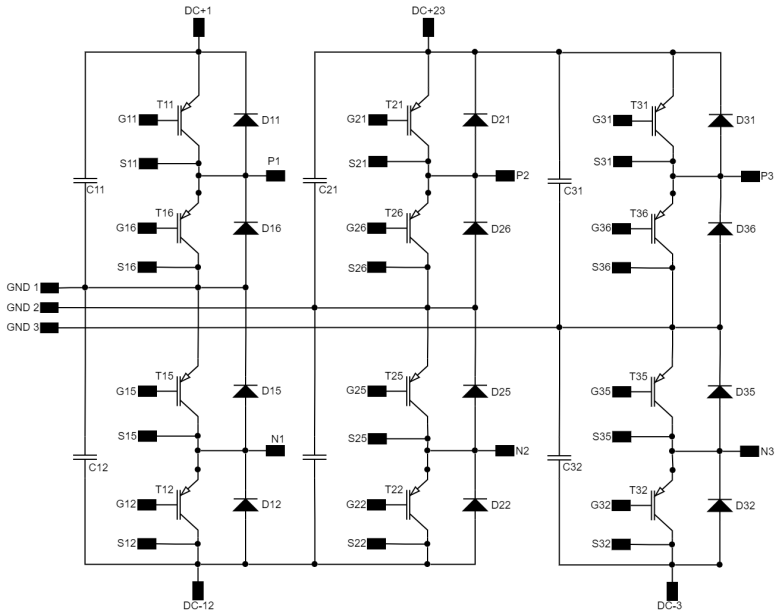

Figure 2.2: DC/DC converter schematics [36]

Component failure is the primary failure mode of DC/DC converter, but assembly failure can also cause the failures. Generally, component failure is caused by electrical overstress. However, environmental factors such as humidity and contamination can also induce failure to DC/DC converter. Assembly failures such as poor wetting in solder joints or migration between solder joints can also result in the DC/DC failure modes [35].

2.1.3 Battery Thermal Management System (BTMS)

Temperature significantly impacts the degradation rate, safety, and life cycle of Li-Ion battery [37]. Therefore, BTMS is required for various purposes, including mitigating thermal runaway and longstanding battery cell lifetime. BTMS can attain and lengthen the lifetime of BESS by retaining the temperature at an optimum level and eliminating substantial heat generated in the battery pack and power converter devices [38]. Various cooling methods, such as air cooling, Phase Change Materials (PCM), straight liquid cooling, ancillary liquid cooling, or fin cooling [38], can be selected.

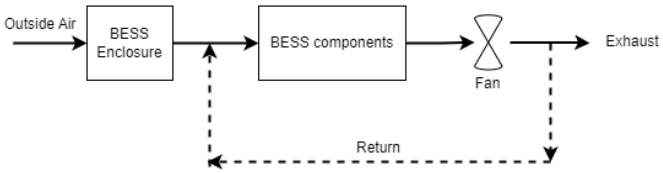

Figure 2.3: Air cooling principle [38]

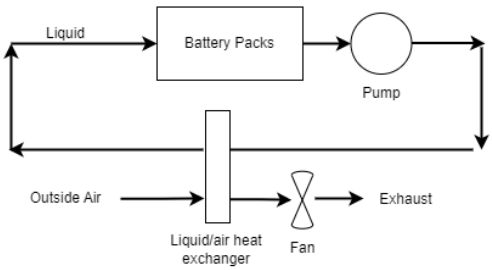

Figure 2.4: Liquid cooling principle [38]

Chacko et al. [39] evaluated the performance of tortuous liquid cooling on the battery pack and concluded that this technique is one of the most promising techniques for battery BTMS. However, the air cooling technique is the most used BTMS for battery cooling due to the lower production cost, energy dissipation, and weight [38][40]. Experimental test data from [41] shows that temperature rises from 25°C to 45°C halves the battery cell cycle life. Another research [42] shows that performing liquid cooling systems enable the reduction of battery capacity loss and resistance growth rate. Another study by Yukses et al. [43] emphasises that applying an air-cooling system BTMS can double the battery life expectancy compared to no BTMS.

The main component of the air cooling system is the fan, while the main component of the liquid cooling system is the pump, fan, and liquid/air heat exchanger [38]. The main components and principals of air cooling and liquid cooling can be seen in Figures 2.3 and 2.4, respectively.

2.1.4 Electrical Protection Devices

2.1.4.1 Molded Case Circuit Breaker (MCCB)

MCCB is used to protect the connection between BESS and the loads. MCCB consists of three main subsystems: the trip elements (thermal-magnetic or electronics), operating mechanism, and arc extinguishers. MCCB protects

the electrical circuit from critical conditions such as short circuits, overload, or earth faults [44]. The mechanism of a circuit breaker must perform six functions: on, off, reset, trip, over travel, and contact reset [45]. Failure on MCCB can be costly and hazardous; therefore, it is important to assess and improve the reliability of MCCB mechanism [44].

The degradation of MCCBs depends on various factors such as the quality of equipment, operating conditions (loading stress, maintenance strategy and practice), and environmental conditions (ambient temperature, humidity, pollution level, etc.) [46]. Jeong et al. [47] conducted a statistical life-span prediction of aged low-voltage breakers, including earth leakage breakers and MCCBs. From 164 MCCBs samples collected and analysed in the study, they concluded that the MTTF of the MCCBs is about 22.78 ± 0.89 yr. A gage repeatability and reproducibility study by Greegory Mathew and Santosh B.Rane [45] concludes that an MCCB can survive minimum $10\,000$ cycles without any performance loss. It can be seen that MCCB is a highly reliable device and requires minimal maintenance [48]. Moreover, mechanical service life (switching cycles) of MCCBs are typically given in the datasheet; this can be used as a reference of MTTF prediction.

2.1.4.2 Direct Current Protection Module (DCPM)

DCPM protects and disconnects the battery packs from the system when failures happen. DCPM mainly consists of fuses and contactors. Fuses provide over-current protection of the electrical circuits. Fuses are appropriate for DC system protection due to their high performance, small dimension, low price, reasonable current limiting characteristics, high breakdown voltage, and high reliability [49]. A fuse is a sacrificial device blown when an over current occurs [50] and must be replaced after abuse. Therefore, it is excluded from the DCPM reliability model.

A contactor is a low-voltage electrical device that can open or close the primary circuit by controlling the coil in the auxiliary circuit [51]. Opening contactors can be performed to ensure the battery packs are continuously operated within safe operating conditions and immediately disconnected from the load when a failure occurs [50]. Contactors in DCPM is controlled by the BMS.

2.1.5 Dry-Type Power Transformer

A power transformer commonly consists of primary and secondary windings connected by a magnetic core or a circuit. When an alternating voltage is

applied to one of the windings (usually the primary winding), there is a flow of alternating current, which generates varying flux in the core. The varying flux induces alternating voltage in the other winding [27][52].

The dry-type transformer is widely used in urban areas due to its non-flammable properties. Moreover, being air-cooled, a dry-type transformer needs less space than the Oil Impregnated Paper (OIP) transformer with the same power rating. The dry-type transformer is not equipped with a radiator bank, which makes it easy to terminate bus work in any location [53]. For a mobile BESS, a dry-type transformer is selected due to its advantages and the possibility of placing it in the same enclosure with electrical load and power electronics. A dry-type transformer is commonly reliable and maintenance-free [54]. It is also considered the safest and most reliable type of transformer in low voltage usage, making it suitable for high safety requirements installation [55]. Same with OIP transformer, the insulation of a dry-type transformer declines due to TEAM stresses, resulting in the insulation materials ageing [53][56]. The failure modes of dry-type transformers are presented in Table 2.2.

In a normal operating condition, the insulation lifetime of a transformer is 180 000 hours [57]. Another reference [55] suggests that the lifetime of a dry-type transformer in nominal working conditions is approximately 110 000 hours; this is consistent with other literature [58][59]. According to Institute of Electrical and Electronics Engineers (IEEE) Guide for Loading Dry-Type Distribution and Power Transformers [60], average lifetime of a transformer at 140°C, 175°C, and 210°C Hottest-Spot Temperature (HST) in a 30°C ambient temperature for 80°C, 115°C, and 150°C temperature rise is 20 years.

Failure Categories	**Failure Mode**	**Consequences**
Mechanical faults	Core steel displacement during construction, DC magnetism, construction faults, transient voltages, and transformer movement	Efficiency reduction, short circuit, and insulation failure
Insulation faults	HST rise, Copper Sulfide production, overloading, unbalanced load	Short circuit and insulation failure

Table 2.2: Dry-type transformers failure modes [27][61]

2.1.6 Software

BESS consists of numerous modern electronic systems that apply significant software usage. The software reliability prediction must be included to achieve a complete reliability evaluation. However, empirical test data is often not available at the moment when a reliability prediction is required. Reliability Information Analysis Center (RIAC) 217Plus™ proposed a software reliability prediction model that does not require empirical data; the model is discussed in Section 3.3.2.1.

Software failure modes are rather complex due to the time dependencies. A single signal mistake in input or output time sequence can create whole software confusion. Common time-sequence failures modes, such as signals being too early, too late, overtime, or frequency abnormality, is quite significant [62]. The failure modes of software are summarised in Table 2.3. Documenting and accumulating different failure modes can be a helpful support to advance the software reliability [62] of BESS.

Failure Categories	**Failure Modes**
Time-sequence input	Data/signal is too early, data/signal is too late, data/signal is overtime, data/signal has frequency abnormity.
Data input	Misplaced and reversed data, redundant data, the deficit of data, data precision error, data is out of range, data error format, refused right inputs, right data range but the wrong value.
File input	Wrong file name, invalid file name, the file does not exist, the file is opened, wrong file format, invalid file format, error file head, error file ending, wrong file length, lack of right information in the file data, blank file context, wrong file data information.

Table 2.3: Software failure modes [62]

2.1.7 Electronics Boards

Electronics boards are essential parts of the BESS since it contains various boards used for control, management, or safety of the BESS operation [63]. Failures of an electronic board can lead to unplanned downtime and revenue loss of the system [63]. Electronics boards consist of Printed Circuit Boards (PCBs) and Surface Mounted Components (SMCs). It means that operating and non-operating temperatures, as well as duty cycle and power cycle rate, impact the reliability of the power electronics boards.

Morries et al. [63] conducted research to predict the electronics board reliability for motor drives under varying application and environmental conditions. The study is based on the RIAC 217Plus^{RM} prediction standards and historical failure data of the PCB and SMCs under analysis. A Monte Carlo simulation was performed to compare the accuracy of the prediction. It is concluded that the RIAC 217Plus^{RM} prediction standards were sensitive to the operating and environmental conditions. However, Monte Carlo simulation using the Probability Distribution Function (pdf) of temperature and operating stresses results in a lower error. Shu et al. [64] conducted a reliability study of electric vehicle batteries consisting of battery system modules and connectors, BMS controller, power devices, and signal detection components. The failure rate prediction is conducted based on the US Navy Mechanical Reliability Estimation Procedures Manual [65], IEC TR 62380:2004 [66], and MIL-HDBH-21 7[67].

2.2 Related Work on BESS Reliability Analysis

Many research papers [6][68][69][70][71] have studied the reliability analysis of the BESS battery packs, which mainly focused on evaluating the reliability of battery packs under different configurations and operating conditions. An operational reliability modelling and assessment of BESS based on Li-Ion battery lifetime degradation has been conducted in [6]. Some studies have been done to assess the reliability of BESS, such as discussed in [2][3][7][72].

A novel Li-Ion battery model was proposed in [6] to diagnose the degradation rate of the film formation of solid electrolyte interphase and the capacity plummeting. A reliability assessment of the Li-Ion battery is then conducted using the Universal Generating Function (UGF). Using the entropy weight method, the resulting reliability importance index is used as the base of the weak-link analytical approach to evaluate the state-oriented and state-change-oriented indexes. The study provides a deep analysis of the Li-Ion battery modelling and reliability analysis of its performance.

A reliability evaluation of large scale BESS has been studied in [2]. The battery modules and power converter are included in the analysis. The reliability analysis of the battery module is based on the State of Health (SOH) of the individual battery cells, which is computed using the weighted Ampere-hour throughput method. The UGF method is also used to analyse the reliability of the battery modules. Different configurations of classic

BESS and Reconfigurable Battery Energy Storage System (RBESS) were also explored. Moreover, the reliability of the power converter is analysed based on the power losses of its semiconductor devices, which are also studied in [73].

A similar method to estimate the SOH levels of the battery pack is performed in [69][74], while the UGF method is also used in [70][71] to compute the reliability of battery pack. Those studies mainly focused on the battery packs and converter; further research is needed to consider other BESS components, such as BTMS, transformers, circuit breakers, electronics boards, or protection systems. Moreover, including the software in reliability evaluation is important to represent the overall BESS accurately.

Chapter 3

BESS Reliability Analysis Method

3.1 Reliability Prediction Methodology

The reliability of an item is the ability to perform a desired function under given conditions and time intervals [75], which often is expressed as a probability [76]. Reliability is critical to high performance since it significantly affects performance, life cycle cost, and economics. Low reliability can trigger increased warranty costs, liabilities, and repair costs [77]. To express reliability as a probability, several functions below are applied in the analysis:

- The *Cumulative Distribution Function (cdf)*, $F(t)$ denotes the probability that an item/system will fail sometime up to time t. This is also called the unreliability function [76][77].
- The *reliability* or *survivor* function, $R(t)$, denotes the probability that an item/system has survived until time t, which can also be calculated as $R(t) = 1 - F(t)$ [76][77].
- The *p-level quantile*, denotes the value t_p, such that $F(t_p) = p, \quad 0 < p < 1$. The *median* denotes the quantile when $p = 0.5$. The $100p$th percentile of time to failure denotes the point at which the probability of an item/system failure equals p. An example of this usage is the B_{10} life of mechanical components usually quoted by manufacturers. B_{10} value is the time at which 10% of components are expected to fail [77].
- The pdf, $f(t)$, is the derivation of $F(t)$ or $-R(t)$, it demonstrates the density of entire possible scenarios [76] .

- The *failure rate* or *hazard rate*, $z(t)$, denotes the (conditional probability that an item/system fails in a small time interval, given that it survived from $t = 0$ until the commencing of the time interval) [77]. $z(t)$ can be expressed with relation to other probability measures as given by Equation (3.1) [76][77].

$$z(t) = \frac{f(t)}{R(t)} \text{ or } R(t) = e^{-\int_0^t z(u)d(u)} \tag{3.1}$$

The failure rate represents changes in the failure probability of an item/system over its lifetime. In practice, the failure rate often exhibits a bathtub shape and is named the *bathtub curve*. Figure 3.1 shows a bathtub curve, and it indicates the phases of failure rates over the product lifetime [76][77].

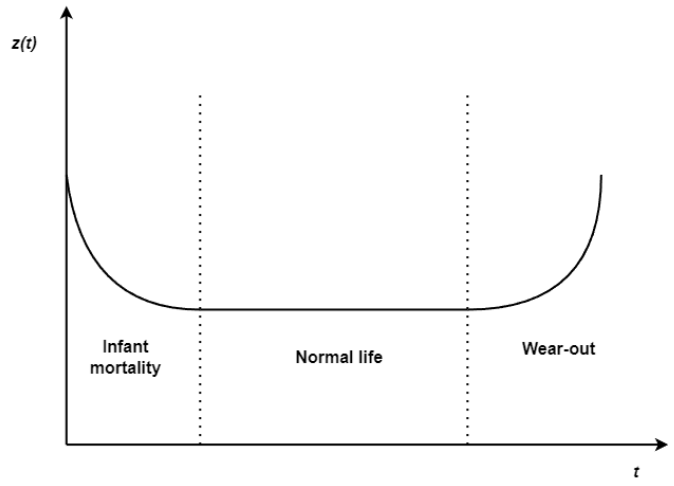

Figure 3.1: Typical bathtub curve [77]

There are three phases in Figure 3.1. The *infant mortality/initial phase* region exhibits a decreasing failure rate; this early failure is commonly due to design, manufacture, or construction defects. The *chance-failure/normal life* region exhibits a constant failure rate with random failures. The reliability analysis is often performed during this phase. The *wear-out/last stage* region has an increasing failure rate, mainly due to ageing phenomena [76][77]. Many reliability analyses assume that the product is in the normal life region. Therefore, the failure rate is considered to be a constant value. Considering a constant failure rate, the reliability function is given by Equation (3.2) [76] :

$$R(t) = e^{-\int_0^t z(u)d(u)} = e^{-\lambda t} \tag{3.2}$$

MTTF of a component denotes the time expectation during which the component can perform its function successfully; it is also called the *expected life*. While MTTF is associated with non-repairable components, there is Mean Operating Time Between Failure (MTBF) for repairable components. MTBF illustrates the time between one failure to the next failure [77]. The assumption that all components are non-repairable is often taken to simplify the analysis. Once the failure rate of a component or subsystem is known, MTTF can be calculated using Equation (3.3).

$$\text{MTTF} = 1/\lambda \tag{3.3}$$

For a *series connected* system, the system reliability $(R_s(t))$ and failure rate (λ_s) for N independent units can be determined by Equation (3.4) [77][78].

$$\begin{aligned} R_s(t) = R_1(t) \cdot R_2(t) \cdots R_N(t) = \prod_{i=1}^{N} R_i(t) \\ \lambda_s = \sum_{i=1}^{N} \lambda_i \end{aligned} \tag{3.4}$$

For a *parallel connected* system, the failure of all units will result in a system failure; a success of only one unit is an adequate guarantee that the system will succeed. The cdf and reliability of N independent units in a parallel connected system are given by Equation (3.5) and 3.6, respectively [77][78].

$$F_s(t) = F_1(t) \cdot F_2(t) \cdots F_N(t) = \prod_{i=1}^{N} F_i(t) \tag{3.5}$$

$$R_s(t) = 1 - F_s(t) = 1 - \prod_{i=1}^{N} [1 - R_i(t)] \tag{3.6}$$

$$\lambda_s(t) = \frac{\lambda_1 \exp(-\lambda_1 t) + \lambda_2 \exp(-\lambda_2 t) - (\lambda_1 + \lambda_2) \exp\left[-(\lambda_1 + \lambda_2)t\right]}{\exp(-\lambda_1 t) + \exp(-\lambda_2 t) - \exp\left[-(\lambda_1 + \lambda_2)t\right]} \tag{3.7}$$

For a system composed of two parallel units, the total failure rate $(\lambda_s(t))$ can be computed using Equation (3.7) [77].

3.2 Battery Packs

3.2.1 SOH Estimation of a Battery Cell

The SOH quantifies the capacity fade or capacity degradation for the battery cell. SOH depict the present battery capacity percentage compared to the original capacity [74][79], given by Equation (3.8) [2][74][79].

$$\text{SOH} = \frac{Q_{current}}{Q_{ini}} = \frac{Q_{ini} - Q_{fade}}{Q_{ini}} \tag{3.8}$$

Where $Q_{current}$, Q_{fade}, and Q_{ini} are the maximum charge capacity of the aged battery cell/pack, the capacity fade or loss of the battery cell/pack, and the total charge capacity of the new battery cell, respectively. When the battery SOH falls to a certain level of threshold value (α), the battery is considered to reach its End of Life (EOL) and categorised as a failed component [2][6].

There are three approaches to calculating the capacity fade of a battery cell/pack in the past [80]: 1) Physicochemical ageing model; 2) Weighted Ah throughput ageing model; and 3) Event-oriented ageing model. The first model offers high precision and detailed information but demands considerable complexity and long calculation time. Another drawback of the first model is the limited data sets available. The third model offers high calculation speed but significantly lower precision results. The second model provides a suitable trade-off between acceptable precision and reasonable calculation time [2]. The Ah throughput ageing model is then selected to estimate the SOH in this study. This ageing model applies the assumption that under stable operating conditions, a battery cell can produce a specific quantity of energy throughput, equal to the charge/discharge cycles number, before reaching the EOL [2][69][80]. Ageing mechanism results in the degradation of Li-Ion battery, which impacts the residual capacity loss and increases the internal impedance, causing degeneration of overall Li-Ion battery performance and reliability [81][82].

The SOH of a battery cell can be calculated using Equation (3.9) [2][69].

$$SOH = SOH(0) - \frac{1}{2 \cdot N_c \cdot Q_{ini}} \cdot \int_0^t |P_B(\tau)| d\tau \tag{3.9}$$

$SOH(0)$ is the initial SOH of a battery cell which equals to 1 for a new

battery. N_c and P_B are the total numbers of cycles before EOL and the battery cell's/pack's power in the particular operating condition [2][69]. The factor 2 in the denominator of Equation (3.9) accounts for integrating both charging and discharging power [69].

The capacity loss ΔQ_{fade}, concerning the initial capacity, can be modelled based on the Arrhenius Equation, it is given by Equation (3.10) [2][37][69][74][79].

$$\Delta Q_{fade} = \frac{Q_{fade}}{Q_{ini}} = B(c) \cdot \exp\left(\frac{-31\,700 + 370.3 \cdot c}{R \cdot T}\right) \cdot (Ah(c))^z \quad (3.10)$$

$B(c)$ and $Ah(c)$ are the pre-exponential factor and the total throughput [ampere-hour] with respect to c, respectively. $B(c)$ is given in Table 3.1 [69][79]. c is the charge/discharge rate, R is the ideal gas constant (8.31 J/mol · K), T is the lumped cell temperature (313 K/40 °C), and z is the power-law factor (0.55) [2][69][79].

c	0.5	2	6	10
$B(c)$	31 630	21 681	12 934	15 512

Table 3.1: The pre-exponential factor [69][79]

To obtain the expression for $N_c(c)$, the energy throughput $Ah(c)$ is first solved using Equation (3.11).

$$Ah(c) = \left[\frac{\Delta Q_{fade}}{B(c) \cdot \exp\left(\frac{-31\,700 + 370.3 \cdot c}{R \cdot T}\right)}\right]^{1/z} \quad (3.11)$$

$N_c(c)$ is then given by Equation (3.12).

$$N_c(c) = \frac{U_B \cdot Ah(c)}{Q_{ini}} \quad (3.12)$$

U_B is the open circuit voltage of a battery cell [V]. c can be computed using Equation (3.13).

$$c = \frac{I_B}{C_B} = \frac{P_B}{U_B \cdot C_B} = \frac{P_B}{Q_B} \quad (3.13)$$

C_B and Q_B are the capacities of the battery cell in Ah and kWh, while I_B is the charge/discharge current. Equation (3.9) can be expressed by Equation (3.14).

$$SOH = SOH(0) - \frac{|P_B|}{2 \cdot N_c(|P_B|) \cdot Q_{ini}} \cdot t \tag{3.14}$$

3.2.2 UGF and Battery Packs Reliability

It is difficult to precisely measure the capacity of Li-Ion battery during the actual operation [6]. The normal distribution is usually used to represent the probabilistic capacity distribution of Li-Ion batteries [2][6]. The battery module failure is defined when its performance is less than the required performance, even though all the battery cells are working [2]. Many functions in reliability modelling generate the same values for different combinations of arguments. In the case of recursive calculations, simplification techniques can reduce the computational burden associated with complex pdf computation [83].

If one separates the degradation process of a battery cell, various states of the battery degradation process can appear; therefore, the system is evaluated as a Multi-State System (MSS). The UGF can be used to analyse the reliability of a MSS [84], such as in this study. UGF make it possible for one to compute the entire MSS performance distribution based on the pdf of individual items using algebraic procedures [84]. The probability of each cell's SOH in each stage after a certain number of cycles can be analysed from the corresponding pdf of each cell's SOH [70]. To analyse the reliability of the battery module with a specific configuration, the UGF method to estimate the reliability of the battery cell has been published in [2][6][70][71].

The SOHs calculated by Equation (3.14) are used to determine the mean SOH (μ), with the variance (σ) is assumed to have linear relationship with μ, so that $\sigma = (1 - \mu)/6$ [2][6][70]. Then, the SOH of the battery cell can be divided into SL different levels, for example, 90% - 100%, 80%-70%, and so on. An array $g = g_1, g_2, ..., g_{SL}$ represents all the battery SOH levels. It also means that there is an assigned value g_l for each range of SOH level $[g_{l-lower}, g_{l-upper}]$. The probability of the SOH falling in the level of g_l is q_l. An array of q_l is $q = q_1, q_2, ..., q_{SL}$, sum of q_l must be equal to 1. The SOH-based UGF of a battery cell is defined by Equation (3.15) [83].

$$U_{SOH}(z) = \sum_{l=1}^{SL} q_l \cdot z^{g_l} \tag{3.15}$$

Assuming that the SOH of a battery cell follows **normal distribution** $N(\mu, \sigma^2)$, q_l can be calculated from the cumulative distribution function $F(t)$

from the normal distribution $N(\mu, \sigma^2)$, with $g_{l-lower}$ and $g_{l-upper}$ are the lower and upper bounds of g_l, respectively.

$$q_l = F(g_{l-upper}) - F(g_{l-lower}) \tag{3.16}$$

To use the UGF method, the following operator needs to be introduced:

$$\Omega(U_{SOH,i}(z), U_{SOH,j}(z)) = \sum_{i=1}^{SL} \sum_{j=1}^{SL} q_i q_j z^{f(g_i, g_j)} \tag{3.17}$$

The vector function $f(g_i, g_j)$ is used to analyse the series and parallel connection of the battery cells and can be defined as follow:

$$f(g_i, g_j) = \begin{cases} \max(g_i, g_j), \text{cells in parallel} \\ \min(g_i, g_j), \text{cells in series.} \end{cases} \tag{3.18}$$

Using the UGF operation, commutative law and associative law apply to the composition operation. Therefore, the same SOH level can be grouped [2]. Assuming that a battery pack consists of N_p number of parallel strings, with each string consisting of N_s battery cells connected in series, the UGF of one cell string is computed using the series operator in Equation (3.19).

$$U_{string}(z) = \Omega(U_{SOH,1}(z), ..., U_{SOH,Ns}(z)) = \sum_{i=1}^{SL} q_s z^{g_s} \tag{3.19}$$

g_s is the resultant SOH level after the defined series configuration operation, and q_s is the probability that the SOH level falls into the level of g_s. The UGF of a battery module/pack consisting of N_p strings connected in parallel is given by Equation (3.20).

$$U_{pack}(z) = \Omega(U_{string,1}(z), ..., U_{string,N_p}(z)) = \sum_{i=1}^{SL} p_s z^{h_s} \tag{3.20}$$

h_s and p_s are the resultant SOH level after parallel operating, and the corresponding probability of the SOH goes into h_s level. If one defines that the battery cell failure happens when the cell's SOH is less than a required threshold (α), the reliability of the battery cell (R_B) can be estimated using Equation (3.21).

$$R_B = \Pr\{h_s \geq \alpha\} = \sum_{h_s \geq \alpha} p_s \tag{3.21}$$

α is given by the vendor in the product specification or can be defined by the user (0.6 or 0.8 is a widely used number) [2][6][70].

3.3 Power Electronics Component

3.3.1 Introduction to the Power Electronics Reliability Prediction Method

The reliability of power electronics components had its milestone with the introduction of reliability prediction tools in 1960. *MIL-HDBK-217* and *Bellcore/Telcordia TR-332* are two widely used tools in reliability prediction. Based on those standards, various commercial software has been developed to estimate the reliability of industrial products [8]. In 2004, French industrialists introduced a new reliability prediction method called the Guide 2014: Reliability Methodology for Electronic Systems [85].

A more current replacement of the *MIL-HDBK-217* was published in 2006. The RIAC's "*Handbook of 217Plus Reliability Prediction Models*" or commonly called *RIAC 217Plus*™ provides methodology and models that covers two main elements: *component* and *system-level* reliability predictions. The system failure rate is estimated using component models by calculating the failure rate of each component. The individual component failure rates are summed to evaluate the system failure rate. A methodology called Process Grading Factors (PGF) is used to modify the system reliability estimation with different system-level factors, including the design, manufacturing, parts quality, systems management, Can Not Duplicate (CND), induced, and wear-out [86]. CND is employed to describe the incapability to replicate field failures during the failure evaluations. The RIAC 217Plus™ [87] is used in this project's power electronics failure rate prediction, and a more detailed explanation is given below.

3.3.2 RIAC 217Plus Reliability Prediction Method

In the failure rate prediction based on 217Plus™ [87], several common parameters, called the global parameters, are used for the power electronics failure rate prediction. These global parameters are used for all power

electronics components, and are given below:

- Y = Manufacture year.
- DC = Duty cycle; the calendar time percentage of the system in which the component operates in the operational state.
- T_{AO} = Ambient temperature during operational state [°C].
- T_{AE} = Ambient temperature during non-operational state [°C].
- CR = Cycling rate; the power cycle number per year to which the system is exposed. It is assumed that the system transitions from a non-operating condition to an operating condition at the exact same time when the power is supplied.
- RH = Relative humidity.

The initial assessment failure rates (λ_{IA}) formulas for power electronics components based on RIAC 217plus™ can be seen in Table 3.2 [2][73][87].

The variables used in the formulas in Table 3.2 and their definitions are listed as follows:

- $\pi_G = \exp\left(-\beta(Y - t_d)\right)$ is the reliability growth failure rate multiplier. Where β is the growth constant. t_d is the year when the data was collected in 1993, according to [87].
- $\pi_C = \left(\frac{C}{C_1}\right)^{CE}$ is the capacitance failure rate multiplier for capacitors. With C as capacitance [microfarads], C_1 and CE are constants for specific capacitor types.
- λ_{OB} is the base failure rate in operating condition.
- $\pi_{DCO} = DC/DC_{1op}$ is the failure rate multiplier for the duty cycle during operating conditions. Where DC_{1op} is the constant applied to a specific electronics item.
- π_{TO} = Failure rate multiplier for temperature during the operating condition, which is given by Equation (3.22). Ea_{op} is the activation energy, operating.

$$\pi_{TO} = \exp\left(\frac{-Ea_{op}}{0.00008617}\left(\frac{1}{T_{vj} + 273} - \frac{1}{298}\right)\right) \tag{3.22}$$

Device	Failure rate formula (λ_{IA})
IGBT	$\lambda_I = \pi_G(\lambda_{OB}\pi_{DCO}\pi_{TO}\pi_S + \lambda_{EB}\pi_{DCN}\pi_{TE} + \lambda_{TCB}\pi_{CR}\pi_{DT}) + \lambda_{SJB}\pi_{SJDT} + \lambda_{IND}$
MOSFET	$\lambda_M = \pi_G(\lambda_{OB}\pi_{DCO}\pi_{TO}\pi_S + \lambda_{EB}\pi_{DCN}\pi_{TE} + \lambda_{TCB}\pi_{CR}\pi_{DT}) + \lambda_{SJB}\pi_{SJDT} + \lambda_{IND}$
Diode	$\lambda_D = \pi_G(\lambda_{OB}\pi_{DCO}\pi_{TO}\pi_S + \lambda_{EB}\pi_{DCN}\pi_{TE} + \lambda_{TCB}\pi_{CR}\pi_{DT}) + \lambda_{SJB}\pi_{SJDT} + \lambda_{EOS}$
Capacitor	$\lambda_C = \pi_G\pi_C(\lambda_{OB}\pi_{DCO}\pi_{TO}\pi_S + \lambda_{EB}\pi_{DCN}\pi_{TE} + \lambda_{TCB}\pi_{CR}\pi_{DT}) + \lambda_{SJB}\pi_{SJDT} + \lambda_{EOS}$
Switch	$\lambda_S = \pi_G(\lambda_{OB}\pi_{DCO}\pi_{TO} + \lambda_{EB}\pi_{DCN}\pi_{TE} + \lambda_{TCB}\pi_{CR}\pi_{DT}) + \lambda_{IND}$
Relay	$\lambda_{Rel} = \pi_G(\lambda_{OB}\pi_{DCO}\pi_{TO} + \lambda_{EB}\pi_{DCN}\pi_{TE} + \lambda_{TCB}\pi_{CR}\pi_{DT}) + \lambda_{IND}$
Connector	$\lambda_{Con} = \pi_G(\lambda_{OB}\pi_{DCO}\pi_{TO} + \lambda_{EB}\pi_{DCN}\pi_{TE} + \lambda_{TCB}\pi_{CR}\pi_{DT}) + \lambda_{IND}$
Resistor	$\lambda_{Res} = \pi_G(\lambda_{OB}\pi_{DCO}\pi_{TO}\pi_P + \lambda_{EB}\pi_{DCN}\pi_{TE} + \lambda_{TCB}\pi_{CR}\pi_{DT}) + \lambda_{SJB}\pi_{SJDT} + \lambda_{IND}$
Inductor	$\lambda_{Ind} = \pi_G(\lambda_{OB}\pi_{DCO}\pi_{TO} + \lambda_{EB}\pi_{DCN}\pi_{TE} + \lambda_{TCB}\pi_{CR}\pi_{DT}) + \lambda_{IND}$
Integrated circuit, plastic encapsulated	$\lambda_{IC} = \pi_G(\lambda_{OB}\pi_{DCO}\pi_{TO} + \lambda_{EB}\pi_{DCN}\pi_{RHT} + \lambda_{TCB}\pi_{CR}\pi_{DT}) + \lambda_{SJB}\pi_{SJDT} + \lambda_{EOS}$
Transformer	$\lambda_T = \pi_G(\lambda_{OB}\pi_{DCO}\pi_{TO} + \lambda_{EB}\pi_{DCN}\pi_{TE} + \lambda_{TCB}\pi_{CR}\pi_{DT}) + \lambda_{IND}$

Table 3.2: Predicted power electronics components' failure rates [87]

T_{vj} is the junction temperature, which equals to $T_{AO} + T_R$. T_R is the component temperature rise above the ambient operating temperature (T_{AO}). $T_{vj} = T_{AO}$ for the component without temperature rise.

- $\pi_P = (P/0.29)^{0.39}$ is the failure rate multiplier for resistor, with P denoting the resistor-rated power.
- π_S is the failure rate multiplier, stress.
  - For bipolar transistors , $\pi_s = 0.21 \exp(0.31 V_s)$, and $V_s = V_{CEapplied}/V_{CErated}$.
  - For diodes, $\pi_s = V_s^{2.43}/0.185$ and $V_s = V_{Applied-reserve}/V_{Rated-reserve}$.
- λ_{EB} is the base failure rate, environmental.
- π_{DCN} is the failure rate multiplier, duty cycle – non-operating, given by Equation (3.23). DC_{1nonop} is a constant given in [87].

$$\pi_{DCN} = \frac{1 - DC}{DC_{1nonop}} \tag{3.23}$$

- π_{TE} is the failure rate multiplier, temperature – environment, given by Equation (3.24). Where Ea_{nonop} is the activation energy, non-operating.

$$\pi_{TE} = \exp\left(\frac{-Ea_{nonop}}{0.00008617}\left(\frac{1}{T_{AE}+273} - \frac{1}{298}\right)\right) \tag{3.24}$$

- π_{RHT} is the failure rate multiplier for temperature-humidity, given by Equation (3.25), with RH is the relative humidity.

$$\pi_{RHT} = exp\left(\frac{-Ea_{nonop}}{0.00008617}\left(\frac{1}{T_{AE}+273} - \frac{1}{298}\right)\right)\left(\frac{RH}{0.5}\right)^3 \tag{3.25}$$

- λ_{TCB} is the base failure rate, temperature cycling.
- $\pi_{CR} = CR/CR_1$ is the failure rate multiplier, cycling rate. Where CR_1 is a constant for specific components given in [87].
- π_{DT} is the failure rate multiplier, delta temperature given by Equation (3.26). with DT_1 is a constant for specific electronics components given in [87].

$$\pi_{DT} = \left(\frac{T_{vj} - T_{AE}}{DT_1}\right)^2 \tag{3.26}$$

- λ_{SJB} is the base failure rate for solder joint.
- π_{SJDT} is the failure rate multiplier for solder joint delta temperature.

$$\pi_{SJDT} = \left(\frac{T_{vj} - T_{AE}}{44}\right)^{2.26} \tag{3.27}$$

- λ_{EOS} is the failure rate for electrical over-stress.

The values of parameters used in the Equations in Table 3.2 can be found in [87]. For the case study in this project, the parameters used in those equations are listed in Appendix A.1.

3.3.2.1 Software Failure Rate Model

The predicted software failure rate (λ_{SW}) at month t_i is given by Equation (3.28) [87].

$$\lambda_{SW} = \left(\frac{F_{t_i-1} - F_{t_i}}{730}\right)(DC \times FL \times FA \times AS) \times 10^6 \tag{3.28}$$

Where F_{t_i} is the number of faults remaining at time t_i, which can be computed by Equation (3.29).

$$F_{t_i} = F_0 e^{-kt_i} \tag{3.29}$$

F_0 is the initial defect density given by Equation (3.30). $KSLOC$ is the lines of source code (in thousands), and FD is the fault density, the initial quality measured at the item shipment.

$$F_0 = KSLOC \times FD \tag{3.30}$$

k is the growth rate, given by Equation (3.31). Where t_i is the time (in months) after the software deployment.

$$k = \frac{\ln\left(\frac{1}{DSL}\right)}{t_s} \tag{3.31}$$

F_{t_i-1} is the number of faults remaining at time $t_i - 1$.

$$F_{t_i-1} = F_0 e^{-k(t_i-1)} \tag{3.32}$$

FL is the fault latency: the average number of times a failure is expected to arise before its underlying fault is fixed. FA is the fault activation, which denotes the fraction of the population showing fault activation. AS is the average per cent severity, which is the fraction of disruptive or critical faults to the customers. DSL is the defect stabilisation level at which the software failure rate stabilises relative to F_0.

3.3.2.2 System Level Failure Rate Model

$$\lambda_P = \lambda_{IA}\left(\Pi_P\Pi_{IM}\Pi_E + \Pi_D\Pi_G + \Pi_M\Pi_{IM}\Pi_E\Pi_G + \Pi_S\Pi_G + \Pi_I + \Pi_N + \Pi_W\right) + \lambda_{SW} \tag{3.33}$$

The predicted failure rate of the system level (λ_P) is given by Equation (3.33) [87]. Where λ_{IA} is the initial assessment of the failure rate computed in Section 3.3.2. Π_P is the parts process factor, Π_D is the design process factor, Π_M is the manufacturing process factor, Π_S is the system management process factor, Π_I is the induced process factor, Π_N is the no-defect process factor, and Π_W is the wear out process factor. Each Π_i can be calculated using Equation (3.34).

$$\Pi_i = \alpha_i \left(-\ln\left(R_i\right)\right)^{\frac{1}{\beta_i}} \tag{3.34}$$

R_i is the rating process for the i$^{\text{th}}$ failure cause $(0-1)$ and is given by Equation (3.35).

$$R_i = \frac{\sum_{j=1}^{n_i} G_{ij} W_{ij}}{\sum_{j=1}^{n_i} W_{ij}} \tag{3.35}$$

G_{ij} is the grade for the j$^{\text{th}}$ item of the i$^{\text{th}}$ failure cause (from $0.0-1.0$), from worst to best. W_{ij} is the j$^{\text{th}}$ item of the i$^{\text{th}}$ failure cause weight and n_i is the number of grading criteria associated with i$^{\text{th}}$ failure cause.

Π_{IM} is the infant mortality factor, given by Equation (3.36), where t is the time in year and SS_{ESS} is the screening strength of the screen(s) applied (if any).

$$\Pi_{IM} = \frac{t^{-0.62}}{1.77}\left(1 - SS_{ESS}\right) \tag{3.36}$$

Π_E is the environmental factor given by Equation (3.37), with Δ_T is the temperature change between operating and non-operating periods $(T_{AO} - T_{AE})$ and G is the random vibration magnitude while the system is operating [G_{RMS}].

$$\Pi_E = \frac{0.855 \times \left(0.8\left(1 - e^{\left(-0.065(\Delta T + 0.6)^{0.6}\right)}\right)\right) + 0.2\left(1 - e^{\left(-0.046 G^{1.71}\right)}\right)}{0.205} \tag{3.37}$$

Π_G is the reliability growth factor given by Equation (3.38), where α is the growth constant, which equals to R_i in Equation (3.35) for the reliability growth processes.

$$\Pi_G = \frac{1.12(t+2)^{-\alpha}}{2^{-\alpha}} \tag{3.38}$$

The parameters used for the process grade factors can be seen in Table 3.3.

Π_i	Name	α	β	Default value if R_i is unknown
Π_D	Design process factor	0.12	1.29	0.094
Π_M	Manufacturing process factor	0.21	0.96	0.142
Π_P	Parts Quality process factor	0.30	1.62	0.243
Π_S	Systems Management process factor	0.06	0.64	0.036
Π_N	CND process factor	0.29	1.92	0.237
Π_I	Induced process factor	0.18	1.58	0.141
Π_W	Wear-out process factor	0.13	1.68	0.106

Table 3.3: Parameters for the process grade factors [87]

3.4 Power Electronics Converters

3.4.1 Inverter System

3.4.1.1 IGBT and Diode Power Losses

The inverter is a bi-directional DC/AC power electronics module. This study uses a 3L-NPC topology. A 3L-NPC topology has the major advantage of its possibility to use diodes and IGBTs with breakdown voltages lower than the DC-link voltage. The device with lower blocking voltage produces lower power losses which increase the efficiency [88].

IGBT is a semiconductor switch; therefore, its failure rate depends on its power losses, which are determined by the current flowing through it [2]. The reliability of the IGBT-based inverter is then determined by the battery C-rate (c) and the ambient temperatures [2]. An analytical approach to quantify the failure rates of power electronics converters based on the C-rate is proposed in [2] and implemented in this study.

$$\begin{aligned} P_I &= P_{I-con} + P_{I-swi} \\ &= \frac{1}{2}\left(U_{CE0}\frac{I}{\pi} + r_{CE}\frac{I^2}{4}\right) \pm m \cdot \cos(\varphi)\left(U_{CE0}\frac{I}{8} + r_{CE}\frac{I^2}{3\pi}\right) \\ &+ \frac{1}{\pi} \cdot f_{swi} \cdot (E_{on} + E_{off}) \cdot \frac{U_{DC} \cdot I}{U_{I-ref} \cdot I_{I-ref}} \end{aligned} \tag{3.39}$$

$$\begin{aligned} P_D &= P_{D-con} + P_{D-rec} \\ &= \frac{1}{2}\left(U_{d0}\frac{I}{\pi} + r_T\frac{I^2}{4}\right) \mp m \cdot \cos(\varphi)\left(U_{d0}\frac{I}{8} + r_T\frac{I^2}{3\pi}\right) \\ &+ \frac{1}{\pi} \cdot f_{swi} \cdot E_{rec} \cdot \frac{U_{DC} \cdot I}{U_{D-ref} \cdot I_{D-ref}} \end{aligned} \tag{3.40}$$

The total power loss of an IGBT module (P_I) and a diode (P_D) is given by Equations (3.39) and (3.40), respectively [2][73]. Subscript $_I$ and $_D$ represent IGBT and diode, respectively. The subscribes $_{con}$, $_{swi}$, and $_{rec}$ represent conduction, switching, and recovery, respectively. P_{I-con} and P_{I-swi} are the IGBT's conduction and switching loss. P_{D-con} and P_{D-rec} denote the conduction and recovery losses of the diodes. U_{CE0} and U_{d0} represent the IGBT's and diode's voltage drops. r_{CE} and r_T are the IGBT's and diode's resistance, respectively. E_{on} and E_{off} represent the IGBT energy losses during on-state and off-state, while E_{rec} is the diode's reverse recovery losses. U_{DC} is the DC voltage at the DC side, and I is the output interface's peak phase current which can be calculated using Equation (3.41). f_{swi} is the switching frequency, $\cos(\varphi)$ is the power factor, and m is the modulation index. U_{I-ref} and I_{I-ref} denote the DC voltage at the DC side, the IGBT's reference commutation voltage and current, while U_{D-ref} and I_{D-ref} represent the diode's reference commutation voltage and current [2][88].

$$I = \frac{\sqrt{2} \cdot P_B}{\sqrt{3} \cdot U_l} \tag{3.41}$$

In Equation (3.41), P_B denotes the output power of a battery cell under a specific operating condition and U_l denotes the line-to-line AC output voltage of the power electronic converter module, which under linear modulation can be estimated using Equation (3.42) [2].

$$U_l = \frac{\sqrt{3} \cdot U_{DC} \cdot m}{2\sqrt{2}} \approx 0.612 \cdot U_{DC} \cdot m \tag{3.42}$$

The modulation index (m) can be estimated using Equation (3.43). U_{RMS} is the AC terminal voltage [88].

$$m = \frac{\sqrt{2} \cdot U_{RMS}}{\sqrt{3} \cdot U_{DC}/2} \tag{3.43}$$

3.4.1.2 Junction Temperature

The IGBTs and diodes are mounted on a heat sink with heat dissipation. The junction temperature (T_{vj}) is the sum of the heat sink temperature (T_{AO}) and the ambient temperature rise in the interface (T_R). T_{vj} is given by Equation (3.44).

$$T_{vj} = T_{AO} + T_R \tag{3.44}$$

Where T_R and T_{AO} are given by Equations (3.45) and (3.46), respectively.

$$T_R = (n_I \cdot P_I + n_D \cdot P_D) \cdot R_{CH} \tag{3.45}$$

$$T_{AO} = T_{AE} + (n_I \cdot P_I + n_D \cdot P_D) \cdot R_{TH} \tag{3.46}$$

R_{TH} and R_{CH} are the thermal resistances from the ambient environment to the heat sink and from the junction to the IGBT's/diode's interface case.

3.4.1.3 DC Cooling Fan

The lifetime of an electronic system is limited by its weakest link. The cooling fan has been reported as one of the top ten failures in electronics products [23][89]. In general, the lifetime of a fan is shorter than the lifetime of other electronic components; therefore, multiple fans are often configured in parallel to increase the reliability of the overall system [23].

Mechanical failures in fans consist of bearing failure, cracks in the fan housing, or rotor failure. While electrical failures usually include electronic packaging failures, solder-joint failures, PCB failures, or semiconductor failures [23].

Two metrics are used to evaluate life expectancy: L_{10} and MTTF. L_{10} denotes the lifetime when ten per cent of populations fail under specific test conditions [23]. Cooling fan manufacturers generally use Weibull distribution to estimate L_{10} and MTTF. The pdf of the two-parameter Weibull distribution is given by Equation (3.47).

$$f(t;\theta,\gamma) = \frac{\gamma}{\theta}\left(\frac{t}{\theta}\right)^{\gamma-1} e^{-\left(\frac{t}{\theta}\right)^{\gamma}} \tag{3.47}$$

Where θ and γ are the scale and shape parameters, respectively, at the same time, the cdf is given by Equation (3.48).

$$F(t) = 1 - e^{-\left(\frac{t}{\theta}\right)^{\gamma}} \tag{3.48}$$

$$L_{10} = \theta \left[\ln\left(\frac{1}{1-0.1}\right)\right]^{\frac{1}{\gamma}} \tag{3.49}$$

$$\text{MTTF} = \theta\Gamma\left[1+\frac{1}{\gamma}\right] = L_{10} \cdot \left(\frac{\Gamma\left[1+\frac{1}{\gamma}\right]}{\left[\ln\left(\frac{1}{1-0.1}\right)\right]^{\frac{1}{\gamma}}}\right) \tag{3.50}$$

Based on Weibull distribution, L_{10} can be computed by Equation (3.49). While the MTTF in relation with L_{10} value is given in Equation (3.50).

Industry standards can be used as references for selecting fans. One of the industry standards is IPC-9591 which standardises the fan's performance parameter [90]. The ratio between MTTF and L_{10} depends on γ, which can be assumed based on IPC-9591 or manufacturer's experiences [23]. Given the MTTF [yr], the failure rate of a cooling fan can be calculated using Equation (3.51).

$$\lambda_{fan} = \frac{1}{\text{MTTF}_{fan}} \tag{3.51}$$

As a reference, IPC-9591 has suggested a shape parameter β of 3.0, and ration between MTTF and L_{10} as 1.89 [23][90].

3.4.1.4 Inverter System Failure Rate

The failure rate of an inverter (λ_{INV}) can be determined from the individual failure rate of the components inside it. There is no parallel redundancy in an DC/AC inverter. A failure in a main component triggers the failure of the whole inverter. The reliability of an inverter can be computed as a series network [91], and the inverter failure rate (λ_{INV}) can be estimated using Equation (3.52)

$$\lambda_{INV} = n_I \cdot \lambda_I + n_D \cdot \lambda_D + n_C \cdot \lambda_C + n_{fan} \cdot \lambda_{fan} \tag{3.52}$$

Where n_I, n_D, n_C, and n_{fan} denote the number of IGBTs, diodes, capacitors, and fans in an inverter.

A BESS usually contains multiple power inverters (commonly three for three phase system) where all inverters must operate. Otherwise, the BESS does not perform in the required voltage and power. Therefore, from the reliability perspective, the inverter system consists of n_{INV} number of

inverters that can be treated as a series connection. The failure rate of the inverter system (λ_{INV-S}) is given by Equation (3.53).

$$\lambda_{INV-S} = n_{INV} \cdot \lambda_{INV} \tag{3.53}$$

3.4.2 DC/DC Converter Failure Rate

To compute the predicted failure rate of DC/DC converter, the same methods as used for inverter failure rate prediction in Section 3.4.1.4 can be used. A DC/DC converter module given in Figure 2.2 consists of IGBTs, diodes, and capacitors. The DC/DC converter's predicted failure rate is given by Equation (3.54).

$$\lambda_{DCDC} = n_{I-DCDC} \cdot \lambda_{I-DCDC} + n_{D-DCDC} \cdot \lambda_{D-DCDC} + n_{C-DCDC} \cdot \lambda_{C-DCDC} \tag{3.54}$$

Where $n_{I-DCDC}, n_{D-DCDC}, n_{C-DCDC}$ are the numbers of IGBTs, diodes, and capacitors in the DC/DC module. While λ_{I-DCDC}, λ_{D-DCDC}, and λ_{C-DCDC} are the failures rate of each IGBT, diode, and capacitor in the DC/DC module.

3.5 Electromechanical Components

The failure rates of electromechanical components can be determined using the B_{10} value and the operating cycles per hour (OC) of the devices [92]. The users can specify OC [77][93]. To estimate the failure rate $\lambda_{electromech}$ [f/hr] from the B_{10} value, Equation (3.55) can be used.

$$\lambda_{electromech} = 0.1 \times \frac{OC}{B_{10}} \tag{3.55}$$

Electromechanical components are commonly irreparable [93], the MTTF [hr] of the electromechanical devices can be computed from $\lambda_{electromech}$ using Equation (3.3) [27][92][93].

$$\text{MTTF}_{electromech} = \frac{1}{\lambda_{electromech}} = \frac{B_{10}}{0.1 \times OC} \tag{3.56}$$

Equations (3.55) and (3.56) are used to estimate the failure rates of MCCB and DCPM in the BESS.

3.6 Control Boards

In a BESS, multiple control boards such as BMS or Insulation Monitoring Device (IMD) exist. Control boards consist of PCB and SMCs. Many SMCs exist in each PCB, such as resistors, capacitors, relays, inductors, diodes, transistors, or integrated circuits. It could be hundreds of components that need to be analysed individually.

According to [64][67][87], failure rates of a PCB and SMCs can be predicted by Equations (3.57) and (3.58).

$$\lambda_{PCB} = 5 \cdot 10^{-3} \pi_{tbx} \pi_{cbx} \left[N_{tbx} \sqrt{1 + \frac{N_{tbx}}{S}} + N_{pbx} \frac{1 + 0.1\sqrt{S_{bx}}}{3} \pi_{Lbx} \right] \left(1 + 3 \cdot 10^{-3} \left[\sum_{i=1}^{j} (\pi_n)(\Delta T_i)^{0.68} \right] \right) \tag{3.57}$$

$$\lambda_{SMC} = \sum \lambda_{sbx} + \sum \lambda_{fbx} + (1 + 3 \cdot 10^{-3}) \left[\sum_{i=1}^{j} (\pi_n) i (\Delta T i)^{0.68} \right] \tag{3.58}$$

$\pi_{tbx} = \exp\left(1740 \left(\frac{1}{303} - \frac{1}{273+T_{AE}}\right)\right)$ is a factor representing the temperature influence. π_{cbx} denotes the influence of number of layers, N_{tbx} is the total number of holes, S is the board's surface area, N_{pbx} is the number of tracks. A default value of $N_{pbx} = \frac{\sum N_s + \sum N_f}{2}$, where N_s denotes the number of lines that connect to each component, and N_f denotes the number of lines that connect every hole. π_{Lbx} is the track width's coefficient, while $(\pi_n)i = n_i^{0.76}$ [94], and ΔT_i is the temperature's variation. λ_{sbx} is the failure of SMCs, λ_{fbx} is the failure rates of through holes, and n_i is the number of component i [64].

3.6.1 Battery Management System Controller

BMS controller monitors and manages the battery system. It meters individual cells' current, voltage, and temperature and evaluates the measured data. The measured data is then used to apply a control strategy to prevent abnormal operation, for example, over-discharge, overcharge, or excess temperature of the battery cells [64]. BMS control boards used in [64] are adopted in the case study. BMS consists of master and slave controllers. The SMCs mounted in

both boards, numbers of each component, and individual failure rates are listed in Appendix A.2. The failure rate of each individual component is calculated in [64] using the methods in [65][67][87]. The value in Tables A.5, A.6, and A.7 are used in Equations (3.57) and (3.58) to compute the BMS failure rates.

3.7 Battery Thermal Management System

Forced air-cooling BTMS has been reported to support an adequate cooling system for the high energy density battery systems [95]. A proficient air-cooling BTMS can dissipate excess heat from the battery packs and regulate the maximum operating temperature, to ensure that it remains under a specific threshold. Furthermore, it assures that the temperature variations within the system are maintained within a desired range [96].

Air-cooling BTMS has several advantages, such as direct access to a low-viscosity coolant, compact size with a straightforward structure, lightweight, cost-effectiveness, low maintenance requirement, and considerably high reliability [96]. It is reported that the forced air-cooling BTMS has an expected lifetime of over 20 years [38]. In this project, the BTMS failure rate is then determined from the average BTMS's MTTF from literature. With the known MTTF, the failure rate of the BTMS (λ_{BTMS}) can be approximated using Equation (3.3).

Chapter 4

Cost-Benefit Analysis Method

The lack of adequate information related to the economic characteristics of BESS is a significant obstacle to deployment, feasible business model development, structures of ownership, and regulation strategies [9][97]. Zakeri et al. [9] studied a comprehensive and comparative review of cost analyses of different Energy Storage System (ESS) systems. To address the varying and dispersed cost data in the available literature, uncertainty analysis was conducted in their research [9].

The life expectancy of BESS significantly impacts the cost analysis [12]. Reliability improvement directly increases the technical lifetime of BESS, which lengthens the economic lifetime and increases revenue. Two main approaches can be used to study the cost of BESS: Total Capital Cost (TCC) and Life Cycle Cost (LCC). TCC investigates all the costs covering purchase, installation, delivery, Power Conversion System (PCS), and Balance of Power (BOP) [9][98].

C_{cap} (€/kW) is the TCC per unit of power rating and can be computed by Equation (4.1).

$$C_{cap} = C_{PCS} + C_{BOP} + C_{stor} \cdot h \tag{4.1}$$

Where C_{PCS}, C_{BOP}, and C_{stor} denote the PCS cost (€/kW), BOP cost (€/kW), and storage compartment cost (€/kWh) respectively. h is the charging/discharging time. The cost elements and explanation of each cost type are given in Table 4.1.

As the owner of the BESS, LCC is an essential indicator for comparing and evaluating different options. LCC covers all the expenditures related to fixed and variable operation and maintenance (O&M), replacement, disposal, and recycling, in addition to TCC [14].

TCC Elements	Costs Elements	Examples
Power conversion system (PCS)	Power interconnections, cabling & piping	Power converter, rectifier
Balance of power (BOP)	Project engineering, grid connection, system integration, BESS isolation & protection devices, construction management, land & access, buildings & foundation, Heating, Ventilation, and Air Conditioning (HVAC) system, monitoring & control, shipment & installation	Switches, DC brakes, fuses, cooling system, voltage & frequency control
Storage section	Containment vessels, construction, & excavation	Battery banks

Table 4.1: TCC elements of BESS [9][99]

The majority of available references reported the ESS costs based on TCC due to the notion that LCC analysis only can be adequately performed with the availability of long-term usage and field experiences data [9]. However, performing LCC analysis is interesting for BESS owners. It can be done by making reasonable assumptions for the unknown parameters, for example, the price of a specific component and maintenance cost reduction due to the increase in reliability. The advantage of LCC is that it enables to set the level of simplifications depending on the analysis purpose [76].

The LCC analysis will be performed using the NPV method. This method can be applied to evaluate and compare capital projects or financial products with the cash flows spread over time. The base of the NPV method is discounting, in which we have to move the cash flows in time. The NPV then can be calculated using Equation (4.2):

$$\text{NPV} = \frac{1}{(1+r)^y} \times C_y = \frac{1}{q^y} \times C_y = \text{NPF}(y,r) \times C_y \tag{4.2}$$

Where r is the interest rate decided by the company, $q = (1+r)$, C_y is the economic value after year$-y$, and NPF(y,r) is the Net Present Factor (NPF) of year $-y$, given by Equation (4.3).

$$\text{NPF}(y,r) = \frac{1}{(1+r)^y} \tag{4.3}$$

The sum of all Net Present Sum (NPS) over y years $(C_{NPS}(y,r))$ is given by Equation (4.4).

$$\mathrm{C}_{NPS}(y,r) = \frac{(1+r)^y - 1}{r \times (1+r)^y} \times C_y = \frac{q^y - 1}{r \times q^y} \times C_y = \mathrm{NPS}(y,r) \times C_y \quad (4.4)$$

LCC is the annualised cost of the investment during the entire economic life of the product of the investment, and the total life cycle cost (C_{LCC}) can be calculated

$$C_{LCC} = C_I + \sum_{i=1}^{y} \frac{C_i}{q^i} - \frac{RV}{q^y} \quad (4.5)$$

Where C_I is the initial investment, C_i is the sum of all costs minus any revenue during the year$-i$, and RV is the residual value [76]. To simplify the analysis, C_I is assumed to be equal with TCC$\times$ profit percentage from the manufacturing perspective.

Chapter 5

BESS Reliability Analysis Results and Discussion

5.1 BESS Configuration in the Case Study

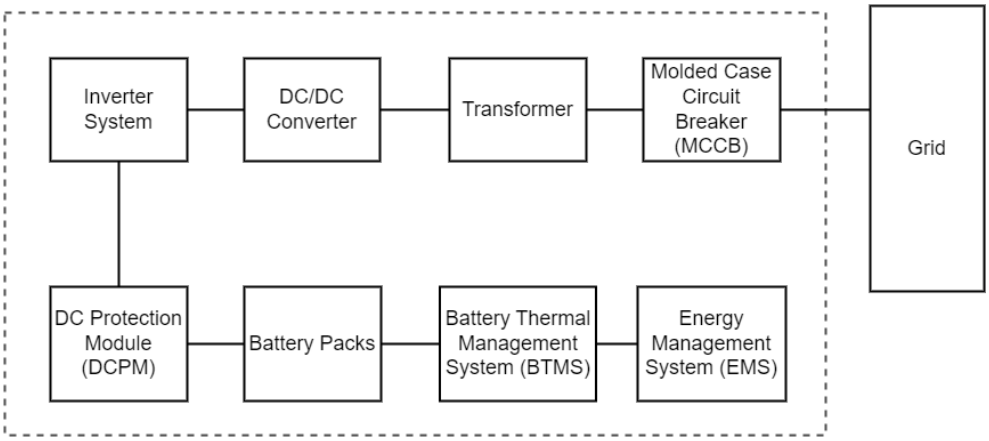

Figure 5.1: BESS topology under the case study, from reliability perspective

Figure 5.1 shows the topology of the BESS under the case study. From a reliability perspective, each fundamental component or subsystem must function well to ensure the operation of BESS. Therefore, all the subsystems' failure rates in Figure 5.1 are computed using the series-connected system approach.

5.1.1 Constant Operating Condition

In reality, a BESS are subjected to fluctuating environmental and operating profile factors; these fluctuations should be simplified in the analysis to keep the research scope reasonable. RIAC 217plus^{TM} [87] suggests default environmental factors for the ground, stationary, and outdoor device, $T_{AE} = 14$ °C, $RH = 50\%$, and 10 G_{RMS} vibration. The normal operating temperature T_{AO} is ser as 40 °C as suggested in [23][96][100]. The case study applies these environmental factors as the constant operating conditions.

While for the power cycles, it is assumed that the BESS is charged/discharged with C-rate $c = 1$ once a week, and $c = 0.5$ twice a day. An equivalent operating condition with duty cycle $DC = 0.3443$ and cycling rate $CR = 730$ are selected to simplify the analysis of the constant operating conditions, with $c = 0.5$.

5.2 Overall Reliability Analysis of BESS

5.2.1 Battery Packs Reliability Analysis

The battery cell is categorised as failed when the performance level is below a specific threshold α. α is usually defined as 0.6 or 0.8, but can be selected based on the manufacturer's recommendation or product specification of a specific battery type [2][6][71]. This case study selected $\alpha = 0.7$ as the mean of $0.6 - 0.8$. The pdf and cdf of the battery cell's SOH using a normal distribution concerning different C-rates (c) are given in Figures 5.2 and 5.3, respectively.

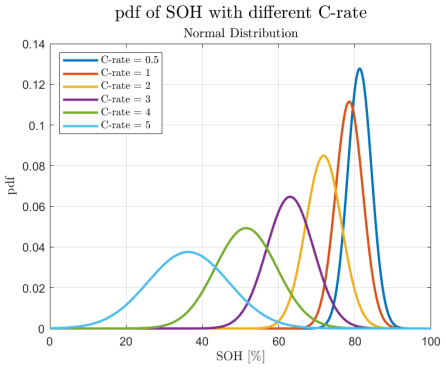

Figure 5.2: pdf of battery SOH

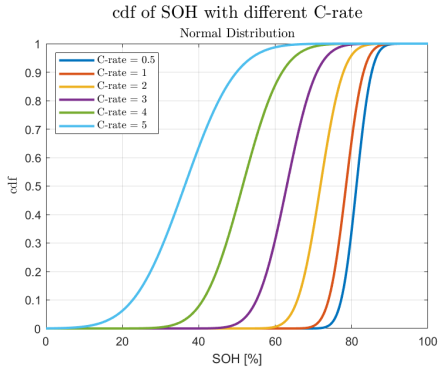

Figure 5.3: cdf of battery SOH

Different c results in different possible cycle numbers before the EOL (N),

which is given in Table 5.1.

c	0.5	1	2	3	4	5
N	3 580	3 125	2 381	1 814	1 383	1 053

Table 5.1: Number of cycles before EOL for different C-rates

It can be seen from Figure 5.2 that the variance increases as the SOH decreases; therefore, lower SOH results in a broader probability distribution. Some parameters strongly affect the SOH of a battery cell, such as operation time, temperature, Depth of Discharge (DOD), and C-rate [69]. Based on Equations 3.12 and 3.14, the battery cell's SOH is impacted by not only the battery power but also the total Ah throughput of the battery cell. The information on Ah throughput with respect to the power levels is vital to study since a very low or very high battery power can not generate an optimum Ah throughput, and BMS is required to improve the battery reliability and optimum Ah throughput of the battery cell [2].

The battery pack configuration from [2] is adopted in this case study; the battery cell and pack specifications are presented in Table 5.2.

Parameters	**Description**	**Cell**	**Pack**
U_B	Nominal voltage	3.3 V	400 V
Q_B	Nominal capacity	20 Ah	200 Ah
Q_{ini}	Initial capacity	66 Wh	80 kWh

Table 5.2: Battery cell and pack specification

The battery system consists of 4 identical battery packs in series connection, each with 10 parallel strings. Each string consists of 121 cells in series. When there is only a series connection between battery cells, the reliability estimation becomes straightforward because the total failure rate of the series connected systems can be easily computed using eq. (3.4). However, with the combination of parallel connections of several strings, the conventional failure rate calculation becomes tedious and not computationally friendly. Fortunately, the UGF approach simplifies the parallel computations, and one can easily estimate the battery packs' reliability regardless of the cells' configurations. The calculation results in the battery system's failure rate of 15.9949 Failures per million hours (FPMH).

5.2.2 Inverter System Reliability Analysis

Based on Figure 2.1, there are 10 diodes, 4 IGBTs, and 4 capacitors in each IGBT module. The parameters used for calculating failure rates of IGBTs, diodes, and capacitors are given in Table A.1. In addition to these parameters, the switching frequency of IGBTs and diodes is 1 MHz, DC voltage at the DC side is $U_{DC} = 650$ V, while the AC terminal voltage is $U_{RMS} = 230$ V.

Temperature rise is a fundamental cause of the degradation in power electronics components. A general rule of thumb quoted in the electronics reliability for capacitors is that each 10 °C temperature rises approximately halves the service lifetime [32]. The change is similar for other semiconductors, but higher temperatures can create slippage [101].

An inverter is usually equipped with active cooling using one or more fans to ensure air circulation for cooling purposes. While for the fan, the MTTF of the fan is commonly given in the datasheet; therefore, the failure rate can be calculated based on the duty cycle (DC) and MTTF, with the unit adjusted to FPMH.

After calculation using equations given in sections 3.3 and 3.4.1, the reliability estimate results can be seen in Table 5.3.

Table 5.3: Predicted failure rate of inverter components

Item	**IGBT**	**Diode**	**Capacitor**	**Fan**
λ [FPMH]	0.1337	0.0817	0.0173	0.7027

Using Equations (3.52) and (3.53), with $n_I = 4$, $n_D = 10$, $n_C = 4$, and $n_{fan} = 1$ for each inverter, and considering there are $n_{INV} = 3$ inverters connected in series (from reliability perspective) in the inverter system, the failure rate of the inverter system is $\lambda_{INV-S} = 6.3693$ FPMH.

5.2.3 DC/DC Converter Reliability Analysis

The DC/DC converter uses heat sinks for thermal cooling [102][103]. A similar method to the previous section about inverter analysis can be implemented to evaluate the reliability of the DC/DC converter. The only difference is that for the doesDC/DC converter, there is no fan as the active cooling since the DC/DC converter uses passive cooling with heatsinks. In Figure 2.2, a DC/DC converter consists of 12 IGBTs, 12 diodes, and 6 capacitors is presented. More detailed values of different DC/DC converter's components' parameters are given in Table A.4 in Appendix A.2. The

predicted failure rate of each DC/DC converter component is given in Table 5.4.

Table 5.4: Predicted failure rate of DC/DC converter components

Item	**IGBT**	**Diode**	**Capacitor**
λ [FPMH]	0.0708	0.0720	0.0418

5.2.4 BTMS Reliability Analysis

The study in [37] shows that active cooling performs better than PCM cooling, especially at high ambient temperatures—however, active cooling results in the larger temperature non-uniformity in the air inlet with low velocities. A comprehensive reliability evaluation of BTMS should consider the reliability of individual components, such as the pumps, fans, temperature sensors, or heat exchangers. A comprehensive understanding of BTMS reliability can be attained considering their failure modes and failure rates.

A more practical and straightforward approach is intended for this case study since the focus is the overall reliability analysis of the entire BESS. Therefore, the BTMS reliability is estimated from MTTF reported in research. Madani et al. [38] reported expected lifetimes of different BTMS techniques. Forced air cooling BTMS, selected in the case study, has a life expectancy of over 20 years. Considering the MTTF [yr], the failure rate of the BTMS in FPMH can be computed using Equation (5.1). The duty cycle is not considered in Equation (5.1) since it is not explained in [38], and to account for calendar degradation, the MTTF is kept the same.

$$\lambda_{BTMS} = \frac{10^6}{\text{MTTF} \times 8\ 760} \tag{5.1}$$

This case study's estimated failure rate of the BTMS is 5.7078 FPMH.

5.2.5 MCCB Reliability Analysis

Approximately 72% of the failures of MCCB occur due to electromechanical reasons [44]. Therefore, estimating the MCCB's failure rate is acceptable using Equation (3.55). The $B10$ value for the MCCB in the case study is $6\ 000$. The normal failure rate for a standard 3-phase MCCB is 0.05 FPMH [93]; this can be used as a reference to compare the estimated MCCB's failure rate. Moreover, it shows that MCCB has a considerably long lifetime and

high reliability. To estimate the failure rate of the MCCB in this case study, the operating cycles per hour (OC) need to be determined by use. It is assumed that the MCCB operates for at least 2 cycles per day, resulting in $\lambda_{MCCB} = 1.3889$ FPMH. OC is the only factor the users can set; higher OC will increase the failure rate and decrease the life expectancy of MCCB. The relationship between the numbers of OC and life expectancy of MCCB is given in Figure 5.4.

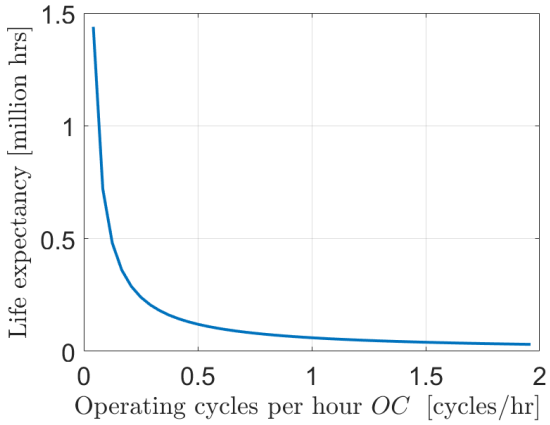

Figure 5.4: MCCB life expectancy for different operating cycles per hour

5.2.6 DCPM Reliability Analysis

The DCPM isolates the battery packs if over-current or over-voltage occurs. The DCPM is modelled as two contactors added with two fuses. As explained in Section 2.1.4.2, the fuses will be excluded from the failure rate prediction since they are sacrificial devices and should be replaced after abuse. Therefore, the failure rate of the DCPM can be approximated as the sum of two contactors' failure rates.

$$\lambda_{DCPM} = 2 \times \lambda_{contactor} \tag{5.2}$$

Like other electrical devices, the life expectancy of a contactor depends on various factors. Those factors vary from the electrical load it is subjected to, the contactor's materials, duty cycle (DC), the surrounding environment, over-current, mechanical wear, maintenance and cleaning. Contactors are also electromechanical devices that can be modelled using $B10$ value. The failure rate of the contactors can be computed using Equation (3.55), which considers

the duty cycle (DC). The $B10$ value of each contactor is $1\ 000\ 000$. In the case study, it is assumed that DCPM operates once a week, resulting in an estimated failure rate $\lambda_{DCPM} = 0.1985$ FPMH. Like the MCCB, the life expectancy of the DCPM is decaying exponentially with higher operating cycles. The dependency of DCPM lifetime with the operating cycle per hour is represented in Figure 5.5.

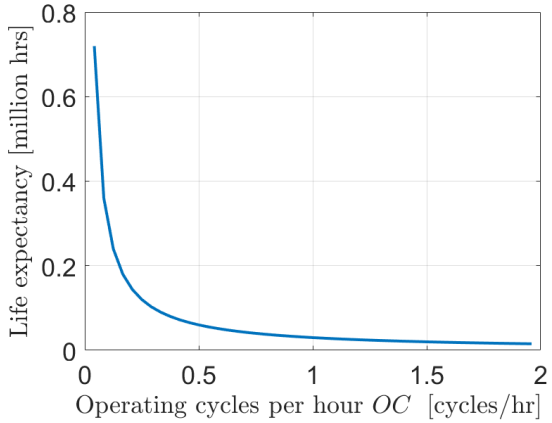

Figure 5.5: DCPM life expectancy for different operating cycles per hour

5.2.7 Transformer Reliability Analysis

The reliability prediction of a transformer is heavily affected by the type of the transformer. For dry-type transformers, the insulation materials affect their life expectancy. The life of transformer insulating materials highly depends on the ambient temperature, temperature rise, and duration of such temperatures. The ambient operating temperature (T_{AO}) highly determines the reasonable load that the transformers can carry. Other factors also impact the insulating materials' life expectancy, such as the electric stress vibration or mechanical stress, reoccurred expansion and contractions, moisture exposure, contaminated environments, radiations, and incompatible materials [104].

Combined with operation time and temperature, the abovementioned factors increase the transformer's thermal degradation and failure rates. The transformer predicted failure rate equations in Table 3.2 combined with Equation (3.33) count the temperatures, environmental impact, duty cycle, cycling rate, manufacturing process, wear out, infant mortality, and vibration, provides relatively simple modelling to estimate the failure rate of

a transformer.

The IEEE Loading Guide Std C57.96™ [60] applied a constant 30 °C hottest-spot allowance for all insulation temperature levels and all size of transformers. While ANSI Appendix C57.96 suggests limiting hottest-spot temperature to 150 °C for ventilated units or 220 °C for sealed units [105]. Basic loading conditions of a dry-type transformer to achieve a normal life expectancy suggested by IEEE Loading Guide Std C57.96™ [60] is explained below:

- The transformer loading occurred continuously at rated kilo-volt-amperes and rated delivered voltage.
- The cooling air average temperature during 24 hours is 30 ° C, and cooling air temperature should never exceed 40° C.
- Altitude of the location does not exceed 3 300 ft (1 005.84 m).

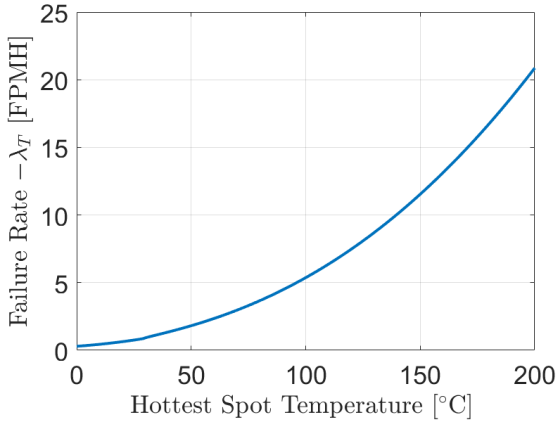

Figure 5.6: Dry-transformer's failure rate - basic loading

Figure 5.6 shows the failure rate of the transformer with the basic loading with respect to the HST. The relationship between dry-transformer HST and the failure rate is not linear since various factors influence the failure rate. The insulation class, materials, loading conditions, and maintenance practice can also affect the dry-transformer failure rate. However, one can conclude from Figure 5.6 that greater HST highly increases the failure rate. Therefore, the existence of a cooling system is a must to lengthen the life expectancy and ensure the reliability of the transformer.

The reliability of dry type transformer is calculated using the methods in Section 3.3.2. Inserting the requirement for the basic loading, the predicted MTTF is $173\,400$ hours or equals to approximately 20 years continuous operation, which is consistent to the literature [55][57][58][59][60]. With the case study duty cycle and cycling rate, the failure rate of the transformer is $\lambda_T = 0.0913$ FPMH.

5.2.8 EMS Reliability Analysis

The EMS plays a vital role in the BESS operation since it monitors, controls, and optimises BESS operation. The EMS typically consists of hardware and software, including control boards and software applications. The control boards act as interfaces between the EMS software and physical components of BESS. The control boards receive measurement signals from different sensors or measurements, control the BESS components' operations, exchange data, and control commands. The EMS software acts as the central intelligence of the BESS operation. It applies different algorithms to monitor, control, and optimise BESS operation. The failure rate of the EMS is the sum of the software's and control boards' (BMS) failure rates.

$$\lambda_{EMS} = \lambda_{SW} + \lambda_{BMS} \tag{5.3}$$

5.2.8.1 Software Reliability Analysis

The Fault Density (FD) and Defect Stabilisation Level (DSL) value based on different Software Engineering Institute (SEI)'s Capability Maturity Model (CMM) level is attached in Appendix A.2. The following parameter values are selected to compute the predicted BESS software failure rate.

The EMS software failure rate is then predicted using Equation (3.28). It is estimated that the BESS software failure rate in this case study is approximately 2.3746×10^{-7} FPMH. It's worth mentioning that industrial software reliability varies greatly depending on various factors. There are different degrees of software complexity and robustness. The EMS software must be tested, validated, and updated continuously throughout the BESS development. Therefore, ideally, the software becomes more mature and reliable over time.

Parameter	Value	Note
$KSLOC$	1 000	Assumption
FD	0.5	See Table A.2
DSL	0.01	See Table A.2
FL	2.0	Default in [87]
FA	1.0	Default in [87]
AS	0.5	Default in [87]
t_s	48 months for an initial software release or 24 months for subsequent release	Default in [87]
DC	0.3443	Based on the case study requirement given in Section 5.1.1

Table 5.5: Software failure rate parameters

5.2.8.2 Control Boards Reliability Analysis

Control boards' reliability predictions depend uniquely on the SMCs attached to the PCBs. Individual components' failure rates must be computed and combined into a system-level failure rate. The case study adopts the same BMS boards used in [64]. This type of BMS boards are available in the market and widely used. However, one can also design and build customised BMS boards for BESS applications.

For this case study, the SMCs and computed individual failure rates are provided in Appendix A.2. To compute the predicted failure rates, the RIAC 217plus™ methods [87] were used in [64]. The BMS failure rate is 5.284 FPMH [64].

In reality, non-operating and operating ambient temperatures, (T_{AE}) and (T_{AO}), impact the predicted failure rate of power electronics components. Fortunately, the BTMS will keep operating ambient temperature below 40 °C. Therefore, one can assume a constant BMS failure rate from the suggested value from [64]. This simplification is also due to the rapidly changing versions of control boards in the BESS that is beyond the scope of this study to consider different versions. One can use the formula in Table 3.2 and methods given in Section 3.3.2 to compute the predicted failure rate of individual power electronics failure rate in the case of another BMS design.

5.3 Overall BESS Reliability Analysis

The minimum required analysis to predict the failure rate for a product or system is the summation of the component-predicted failure rates [87]. The

overall reliability of the BESS in the case study can be predicted using Equation (5.4).

$$\lambda_{BESS} = \lambda_B + \lambda_{INV-S} + \lambda_{DCDC} + \lambda_{BTMS} + \lambda_{MCCB} + \lambda_{DCPM} + \lambda_T + \lambda_{EMS} \tag{5.4}$$

The individual component/subsystem failure rate in FPMH in this case study is summarised in Table 5.6.

Table 5.6: Failure rate of BESS individual component

Item$-i$	**Symbol**	**λ_i [FPMH]**
Battery packs	λ_B	15.9949
Inverter system	λ_{INV-S}	5.5899
DC/DC converter	λ_{DCDC}	1.6518
BTMS	λ_{BTMS}	5.7078
MCCB	λ_{MCCB}	1.3889
DCPM	λ_{DCPM}	0.1985
Transformer	λ_T	0.0913
EMS	λ_{EMS}	5.2840

The reliability of the BESS with respect to the operating hours and its predicted MTTF is given in Figure 5.7.

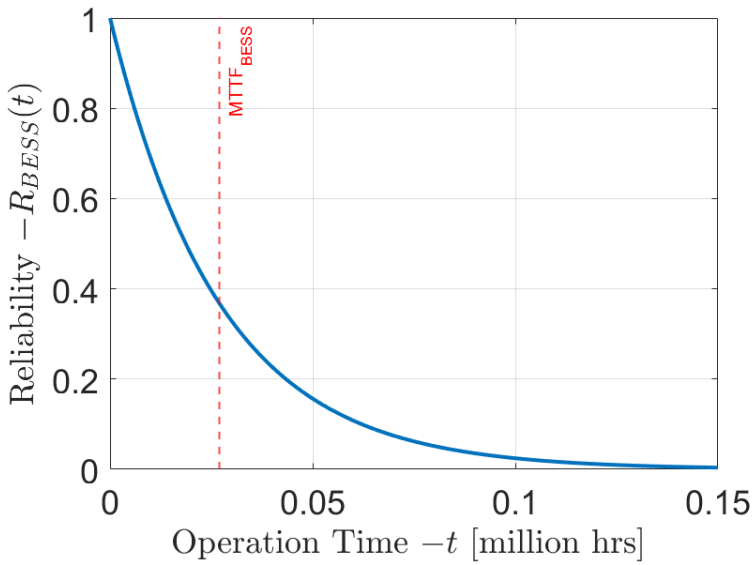

Figure 5.7: Overall BESS reliability

With the operating scenario given in Section 5.1.1, the predicted failure

rate of the BESS is $\lambda_{BESS} = 35.9070$ FPMH, with MTTF of $27\,850$ operating hours.

5.4 Sensitivity Analysis

Sensitivity analysis evaluates how sensitive the model is to the variations of different data and parameters that form its foundation [106]. To understand the influence and impact of different parameters on the overall BESS reliability, sensitivity analysis is performed for different operating ambient temperatures, non-operating ambient temperatures, duty cycles, and charge/discharge rates.

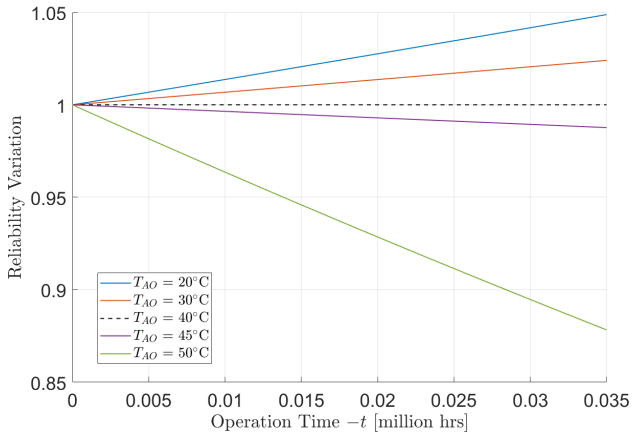

Figure 5.8: BESS reliability difference for different constant operating ambient temperatures

The BESS operating ambient temperature is suggested to be kept below 40 °C using the BTMS. The ideal operating temperature for a battery cell is to keep it below 35 °C; in the minimum temperature, it should be greater than 15 ° C [107]. Figure 5.8 shows that when the operating ambient temperature is above 40 °C, the BESS reliability significantly deteriorated. Using the BTMS and keeping the operating ambient temperature within the safety range is crucial. Otherwise, the degradation of the BESS will rapidly happen.

Environmental stress, such as the non-operating ambient temperature, has a considerable impact on the BESS reliability as well. The non-operating ambient temperature affects the battery cells' electrochemical reactions and internal resistance. Higher temperatures will accelerate the chemical reactions, which can lead to shortened battery cells' life expectancy. On

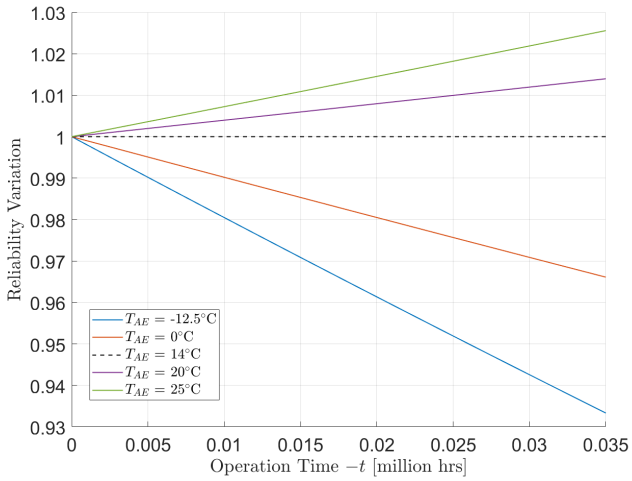

Figure 5.9: BESS reliability difference for different constant non-operating ambient temperatures

the other hand, extremely low temperatures also impeded the battery cell degradation. Figure 5.9 shows this phenomenon. The optimal non-operating ambient temperature is needed.

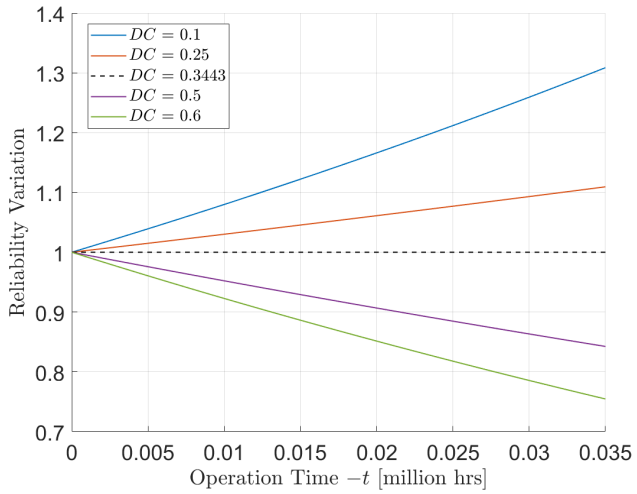

Figure 5.10: BESS reliability difference with respect to different duty cycles

Duty cycle (DC) is a global parameter used for all BESS component mathematical models. It is evident that a higher duty cycle directly accelerates

the degradation and shortened life expectancy of the BESS. Figure 5.10 shows how different DCs affect the reliability of the BESS over time. DC must be considered during the design and the planning of BESS adoption since this will affect the expected lifetime depending on how high the applied DC is.

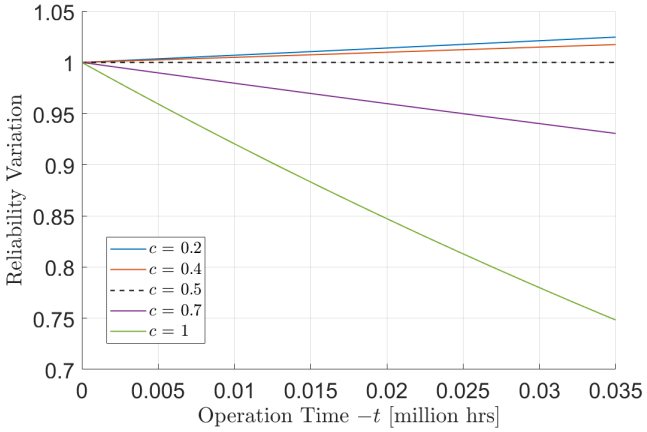

Figure 5.11: BESS reliability difference with respect to different C-rates

Figure 5.11 shows C-rates' influence on the overall BESS reliability. C-rates directly impact battery degradation. High C-rates meaning rapid charging or discharging, can accelerate the degradation mechanism of the battery cells. Accelerated degradation implies the reduction of cycle life and battery reliability. One must select the C-rate based on the desired technical lifetime of the battery. Higher C-rates result in faster degradation due to the voltage drops within BESS. Rapid charging/discharging can increase the battery's internal resistance, increasing capacity loss and reducing battery efficiency.

Quantifying the influence of different variables above using sensitivity analysis helps identify the optimal design or usage strategy. By considering different scenarios and assessing the sensitivity of BESS toward different variables, one can optimise BESS performance, extend the technical lifetime, and maximise the financial profit.

Chapter 6

Navigating the Trade-Off between Reliability and Profitability

To increase the system's reliability, the following options can be done [108][109]: (a) Increase the component's reliability; (b)Apply redundant components in parallel; (c) Use a combination of the component's reliability improvement and parallel redundancy; and (d) Interchangeable components reassignment.

This project focuses on the second option to enhance the BESS reliability. There are two strategies to implement redundancy: the active and standby strategies. In the active strategy, all the redundant components initiate their operation simultaneously from the start, despite only one component being needed at any specific instant [109]. In the standby strategy, redundant components are systematically added to the system following a prearranged sequence of prompts from the mechanism whenever a failure occurs [110][111].

Different scenarios affecting the costs and reliability are analysed from the manufacturing and ownership perspective. First, the original design is explored, followed by other scenarios to improve the reliability of the BESS. For the original design, the initial cost for each subsystem analysed in the BESS is presented in Table 6.1. Different scenarios to improve the BESS reliability, followed by failure rate (λ_{BESS}) and corresponding MTTF are given in Table 6.2. The decrease in failure rate increases the MTTF, which means a longer technical lifetime period for the system to operate. This is essential in analysing the LCC, especially for the customers/owners buying the

system. Further analysis on the TCC from the manufacturing perspective and the LCC analysis from the ownership perspective are presented in Sections 6.1 and 6.2, respectively.

The price of each component is approximated by the average cost available in the literature. The economic analysis from World Bank in 2020 [112] provides most of the capital cost data in this project as capital cost per kWh installed BESS. Table 6.1 presents each system's cost assumption.

Component	**Price**	**Unit**	**Unit Qty**	**Total Price [€]**	**Note**
Battery Pack	122	€/kWh	320	39 040	[113][112]
Inverter	36.08	€/kWh	320	11 546	[112]
DC/DC Converter	700	€/unit	1	700	*
MCCB	2 680	€/unit	1	2 680	*
EMS	17.58	€/kWh	320	5 626	[112]
BTMS	16.73	€/kWh	320	5 354	[114]
Transformer	18.50	€/kWh	320	5 920	[112]
DCPM	1 500	€/unit	1	1 500	*
Total				**72 365**	

**assumption based on market price*

Table 6.1: BESS components prices

Table 6.1 shows that only the cost of each component/subsystem is included in the computation. There are BOP costs such as the project engineering, construction management, shipment and installation are excluded. It is assumed that the costs of the BOP still exist even though the reliability of the BESS is improved. Therefore, the relationship between those BOP costs with reliability is not linear and is not considered in this project.

Scenario	**Note**	λ_{BESS} **[f/yr]**	**MTTF [yr]**
1	Original design	0.1082	9.2
2	Redundancy on the inverter system	0.0924	10.8
3	Redundancy on the battery packs	0.0681	14.69
4	Redundancy on the BTMS	0.0921	10.86
5	Redundancy on the transformer	0.1079	9.27
6	Redundancy on the DC/DC converter	0.1033	9.68
7	Redundancy on the MCCB	0.1040	9.61
8	Redundancy on the DCPM	0.1076	9.30

Table 6.2: Scenarios on redundancy to improve BESS reliability

6.1 Total Capital Cost - Manufacture Perspective

From the manufacturing perspective, the TCC of a BESS system is an important parameter to evaluate. Manufacturers produce and sell the product, and minimising the TCC for optimal reliability is required.

TCC should evaluate all the costs covering purchase, installation, delivery, PCS cost, energy storage cost, and BOP costs [9][115]. For this project, a simplification is taken, and the TCC covers the cost of each subsystem calculated on the reliability analysis. The cost for each subsystem is approximated based on available literature. An approximation based on the average market price is selected in the presence of unavailable data.

The combined failure rate (λ) of redundant components is computed using Equation (3.7). Based on subsystem cost given in Table 6.1 and reliability calculation in Section 5.1, the TCCs and reliability of different scenarios are presented in Figure 6.1. Reliability decreased over time; in Figure 6.1, the BESS reliability in the 2^{nd} year of operation is presented.

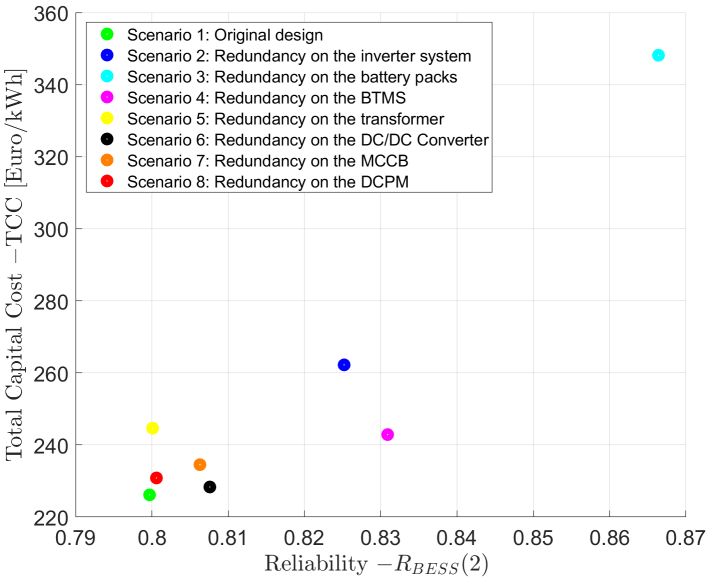

Figure 6.1: BESS TCC, manufacture's perspective

From Figure 6.1, it can be seen that applying redundancy to improve the reliability of overall BESS always comes with an increase in the total

expenses. Even though higher reliability increases the revenue gained for the owner, the original design (scenario 1) has the lowest TCC. Scenario 6 has the second lowest TCC, increasing the reliability by 1%. A similar reliability increase can be achieved by scenario 7 as well. However, scenario 7 has a higher TCC cost than scenario 6. Scenario 5 and scenario 8 do not result in visible reliability increases. This is because transformer and DCPM are highly reliable and have long lifetimes. From a reliability perspective, to give significant reliability improvement, redundancy must be applied to the less reliable component, for example, the battery backs or BTMS in scenarios 3 and 4. However, the profitability of the action must be considered as well. Since battery packs are costly, giving over capacity for the battery packs increases the cost by 54%, which might not be an economically feasible idea. While for the BTMS redundancy, the TCC only increase by 8% and reliability is improved by 4%. The extent of the redundancy must be carefully analysed based on the particular needs of the BESS application.

6.2 Life Cycle Costs - Ownership Perspective

From the ownership perspective, the LCC is a more interesting parameter to evaluate the BESS. The LCC covers all expenses related to operation, maintenance, replacement, disposal, and recycling in addition to the TCC [9]. When performing cost analysis, limiting the battery DOD to 80% is suggested to prolong its life expectancy. Furthermore, it is advisable to acquire replacement when the battery reaches 80% useful lifetime to prevent performance degradation [12]. To evaluate the LCC of the BESS, economic parameters given in Table 6.3 are utilised. Assuming 80% DOD with 2 cycling rate per day, same operating condition as the case study in Section 5.1, the annual electricity production is approximately $186\,880$ kWh/yr.

Parameter	Value	Unit	Note
Interest rate (r)	8	%	[9]
Charging electricity price	0.05	€/kWh	[9]
Selling electricity price	0.16	€/kWh	*
Fixed O&M cost	6.9	€/kW-yr	[9]
Variable O&M cost	0.0021	€/kWh	[9]
Disposal cost	9.25	€/kWh	[116]

**assumption based on market price*

Table 6.3: Economic parameters and assumptions

National Renewable Energy laboratory suggested that 17% profit for the BESS calculation [117]. This margin is applied to all direct costs covering hardware, labour, sales, marketing, design, and permit fees. Only the hardware is considered on the LCC calculation; however, the concept of the computation can be extended if more cost information is available. The expenses can be modelled as negative values, while revenues as positive values in the LCC analysis. In Table 6.4, the investment cost is TCC [€] in Section 6.1 added with 17% margin for the manufacturer.

Scenario	**Investment Cost [€]**	**O&M [€]**	**Residual Value [€]**	**Disposal Cost [€]**	**Lifetime [yr]**
1	846 675	2 600	4 000*	2 960	9
2	98 175	2 502	4 000*	2 960	10
3	130 344	2 375	4 000*	5 920	14
4	90 931	2 502	4 000*	2 960	11
5	91 593	2 600	4 000*	2 960	9
6	854 865	2 568	4 000*	2 960	9
7	87 802	2 568	4 000*	2 960	9
8	86 422	2 600	4 000*	2 960	9

**assumption based on market price*

Table 6.4: Economic parameters and assumptions

With 8% interest rate, using Equation (4.3), the NPF with the economic lifetime up to 14 years are computed in Table 6.5.

Year $-y$	0	1	2	3	4	5	6	7
NPF$(y, .08)$	1	0.926	0.857	0.794	0.735	0.681	0.630	0.583
Year $-y$	8	9	10	11	12	13	14	
NPF$(y, .08)$	0.540	0.500	0.463	0.429	0.397	0.368	0.340	

Table 6.5: NPF year $-y$

In the LCC calculation, the expenses are positive, while the revenues are modelled as negative costs. The annual revenue is decreasing due to the decrease of the annual energy yield, which is modelled with a linear relationship with the battery cell capacity fade (ΔQ_{fade}), or the SOH decrease. Using a 250 kWh initial capacity (Q_{ini}) of the BESS, with 80% DOD and 2 cycling per day, the annual energy production in the year$-y$ (AEP(y)) can be approximated using Equation (6.1).

$$\text{AEP}(y) = (Q_{ini} \cdot DOD \cdot CR) - \left(\frac{\Delta Q_{fade}}{LT} \cdot (Q_{ini} \cdot DOD \cdot CR \cdot y) \right) \quad (6.1)$$

Year$-y$	0	1	2	3	4
NPF(y)	1	0.926	0.857	0.794	0.735
AEP(y)	0	186 880	179 872	172 864	165 856
Investment Cost [€]	84 667	0	0	0	0
O&M Cost [€]	0	2 600	2 600	2 600	2 600
Residual Value [€]	0	0	0	0	0
Disposal Cost [€]	0	0	0	0	0
Charging Cost [€]	0	9 344	8 994	8 643	8 293
Revenue [€]	0	-29 901	-28 780	-27 658	-26 537
Total Cost [€]	84 667	-17 956	-17 185	-16 415	-15 644
NPV(y) [€]	84 667	-16 626	-14 734	-13 030	-11 499

Year$-y$	5	6	7	8	9
NPF(y)	0.681	0.630	0.583	0.540	0.500
AEP(y)	158 848	151 840	144 832	137 824	130 816
Investment Cost [€]	0	0	0	0	0
O&M Cost [€]	2 600	2 600	2 600	2 600	2 600
Residual Value [€]	0	0	0	0	-4 000
Disposal Cost [€]	0	0	0	0	2 960
Charging Cost [€]	7 942	7 592	7 242	6 891	6 541
Revenue [€]	-25 416	-24 294	-23 173	-22 052	-20 931
Total Cost [€]	-14 873	-14 102	-13 331	-12 560	-12 829
NPV(y) [€]	-10 122	-8 887	-7 779	-6 786	-6 418
NPS [€]	**-11 213**				

Table 6.6: Original design's LCC analysis

To demonstrate the LCC analysis, the calculation for the original design is presented in Table 6.6. The details calculations for other scenarios are presented in Appendix B.1. The increase in reliability reduced the maintenance cost. The fixed and variable O&M costs are assumed to be reduced by $28€$ and $5€$ for every 1% reliability increase. In this LCC analysis, expenses are modelled as positive values, while revenues/incomes are modelled as negative values. That means that negative NPS shows that the scenario is profitable.

From Figure 6.2, it can be seen that the improvement in the BESS reliability can lead to either additional or reduction of profit for the BESS owner. An interesting scenario is scenario 4, where the BTMS has a considerably high failure rate and implements redundancy on BTMS, significantly improving the reliability and profitability of the BESS ownership. With only 8% additional investment cost to add BTMS redundancy, the NPV is increased by 27% for the BESS owner. Other scenarios improve the reliability of the BESS but are not worth performing due to the lower profitability. In scenario 3, the redundancy of batter packs makes the investment less profitable. For the owners of BESS, LCC analysis is essential to creating a cost-effective decision. Including more details on the expenses

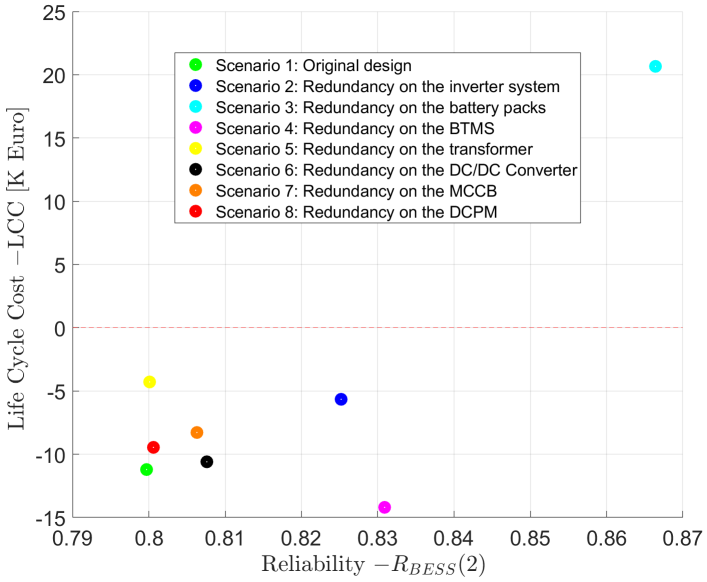

Figure 6.2: BESS LCC, ownership perspective

and revenues can provide more accurate information on the BESS profitability and reliability, making the BESS owner can navigate the trade-off between cost and BESS performance to select the most suitable case.

6.3 Discussion on Cost Optimisation

Evaluating how to improve the reliability and profitability of BESS is necessary to create a decision-making tool to determine the best scenarios for manufacturers or owners [14]. There are various factors to consider when doing LCC analysis. Interest rate (r) is among the most significant factors since different interest rates result in different perceived profitability for the company. Figure 6.3 shows the LCC computation for the 8 BESS scenarios from the ownership perspective.

It can be seen from Figure 6.3 that higher interest rates lower the NPV of future cash flows. Conversely, lower interest rates increased the NPV of future cash flows. Different interest rates result in a different optimum scenario, as seen in Figure 6.3. In this case study, scenario 4 with the redundancy in BTMS stays the most profitable scenario with different interest rates. However, different results can happen in different cases. Therefore, a BESS

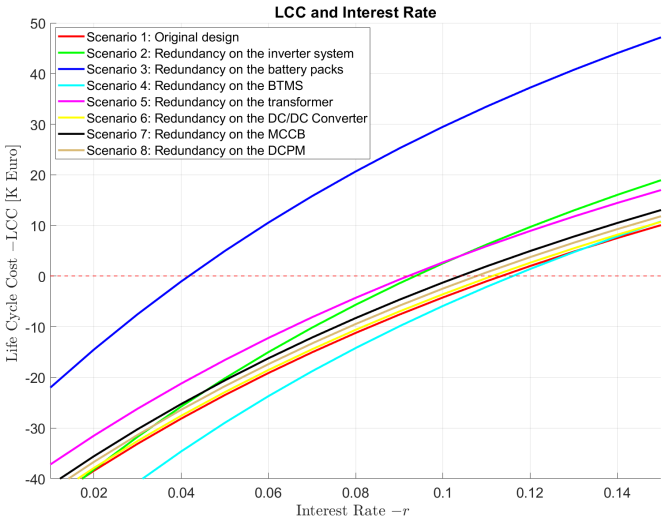

Figure 6.3: BESS LCC with different interest rate

owner should carefully consider the interest rate selection and other economic assumptions. This also applies to the manufacturers or stakeholders in the BESS supply chains. Selecting a balanced trade-off between reliability and costs is crucial for BESS adoption. Since the BESS technology advancement makes the price down over time, assessing the LCC over the technical lifetime is vital to ensure the profitability of the BESS adoption.

Chapter 7

Conclusions and Future work

In this chapter, the conclusions and future work recommendations are given based on the results and discussions presented in the previous chapters.

7.1 Conclusions

The study found that the BESS reliability prediction methods result in reasonable indices to demonstrate BESS reliability. BESS reliability and life expectancy highly depend on the operating conditions and stress factors. Ensuring that the BESS operates within the safe range of operation and environment factors is crucial. The operating temperature, loading current, charging/discharging rate, cycling rate, and duty cycle significantly affect the reliability and life expectancy of BESS. In addition, environmental factors such as relative humidity or vibration also impact the reliability of BESS. There is always a possibility of random failures occurring in a system, which is also difficult to predict. Therefore, monitoring and maintenance are essential to minimise the risk of accelerated degradation.

Case studies have been performed to evaluate the BESS performance when facing different operating and environmental conditions. Several redundancy scenarios and their corresponding cost-benefit analysis were presented to investigate the balance trade-off between reliability improvement and costs. Case studies show that improving the BESS reliability may cause an increase in the total capital cost (TCC). However, improved reliability lengthens the BESS technical lifetime and reduces maintenance costs, which can result in more profitable scenarios. The case study in this project shows that redundancy in BTMS is the most promising scenario since the rise of lifetime and revenue outweigh the additional expenses that come with the redundancy.

Different cases, of course, can result in different profitability since LCC analysis is specific for each case.

Further research and actual tests are required to validate the reliability prediction results. Nonetheless, the findings of this research provide a prediction model for BESS under the design phase and help to predict the outcome of design decisions. The combination of reliability and cost-benefit analysis can help establish the viability of adopting BESS.

7.2 Limitations

To validate the reliability prediction method, historical or experimental data are required. If actual performance data is not possible, experiment effort such as an accelerated test is required. However, it is not conducted in this research. BESS is a relatively new industrial product, and rapid design changes occur over time; available historical data is limited. This limitation makes it difficult to validate the predicted reliability indices. The same limitation also applies to the cost data of each component, where minimal literature is available, and some approximations must be taken, which can affect the accuracy of the computation.

The scope of this research is to get an understanding of overall BESS reliability. Some components are too wide to be considered in detail; therefore, simplifications and results from other literature are adopted. For example, the BMS reliability assessment refers to a research result from [64]. BMS reliability highly depends on the SMCs mounted on it and is very specific for each design. However, a complete methodology that is easy to replicate and scale is provided in this project.

In the cost analysis, only components in the reliability analysis are included. In reality, the TCC of a BESS covers additional costs such as project engineering, construction management, land, access, shipment, and installation costs. Those levels of detail are beyond the scope of this project. However, the same computation methods are applicable if the cost data is more detailed.

7.3 Future work

7.3.1 Accelerated Test

To validate the reliability prediction, real experimental data is needed. An accelerated test can be done to get the real reliability data of BESS. The experimental data can be combined with the predicted reliability indices for more accurate results.

7.3.2 Long-Term Performance Assessment

A reliability prediction method is helpful to predict the BESS reliability during the design phase. Once the product is deployed, a long-term performance assessment must be done to further evaluate the technical and economic viability. This requires continuous monitoring and evaluation of the system's performance.

7.3.3 Deeper Cost-Benefit Analysis

A more detailed cost-benefit analysis shall be conducted to establish a feasible business model for the manufacturer and potential owners. More realistic assumptions, such as real-time electricity price prediction, may be helpful. Actual prices of the components also vary for different brands/designs. Therefore, the cost-benefit analysis is very specific for a specific case. Moreover, the socioeconomic factors that impact the cost-benefit analysis can also be considered. For example, if there are incentive programs to support green energy, such as the carbon tax, guarantee of origin, green energy subsidy, or green certificates.

7.4 Ethical and Sustainability Reflections

The thesis contributes to the United Nations (UN) Sustainable Development Goals (SDGs) numbers 7, 9, and 10 by providing a study and perspective of BESS development. The BESS is a fundamental system enabling global energy transition and reducing carbon emissions. Proposing methods that can be replicated to analyse the reliability and economic feasibility of BESS can provide a tool to other parties that want to evaluate the feasibility of their BESS project. Improving the reliability of the BESS promotes sustainability by increasing efficiencies and reducing waste from BESS materials and

operations. By lowering the failures and need for replacement, fewer material disposals are required. This aligns with the ethical effort to consume responsibly from natural resources. Higher BESS reliability facilitates higher renewable energy penetration and improves grid resilience.

It is worth mentioning that BESS applications can be used for emergency response and rural electrification. Taking advantage of the BESS technology to provide electricity access to the underserved community can help reduce the social gap. Many benefits come with BESS reliability improvement and profitability. Therefore, studies about BESS reliability and cost-benefit analysis must be explored further.

References

[1] Irena, "Global Energy Transition a Roadmap to 2050," Apr. 2018, irena2018. [Online]. Available: https://www.irena.org/publications/2018/Apr/Global-Energy-Transition-A-Roadmap-to-2050?source=post_page---------- [Page 1.]

[2] M. Liu, W. Li, C. Wang, M. P. Polis, L. Y. Wang, and J. Li, "Reliability Evaluation of Large Scale Battery Energy Storage Systems," *IEEE Transactions on Smart Grid*, vol. 8, no. 6, pp. 2733–2743, Nov. 2017. doi: 10.1109/TSG.2016.2536688 Conference Name: IEEE Transactions on Smart Grid. [Pages 1, 6, 8, 15, 20, 21, 22, 23, 24, 25, 30, 31, 41, and 42.]

[3] N. Garimella and N.-K. C. Nair, "Assessment of Battery Energy Storage Systems for Small-Scale Renewable Energy Integration," in *TENCON 2009 - 2009 IEEE Region 10 Conference*, Jan. 2009. doi: 10.1109/TENCON.2009.5395831 pp. 1–6, iSSN: 2159-3450. [Pages 1 and 15.]

[4] M. Qadrdan, N. Jenkins, and J. Wu, "Chapter II-3-D - Smart Grid and Energy Storage," in *McEvoy's Handbook of Photovoltaics (Third Edition)*, S. A. Kalogirou, Ed. Academic Press, Jan. 2018, pp. 915–928. ISBN 978-0-12-809921-6. [Online]. Available: https://www.sciencedirect.com/science/article/pii/B9780128099216000252 [Page 1.]

[5] I. S. Association, "Mobile and Transportable Energy Storage Systems – Technology Readiness, Safety and Operation," Feb. 2022. [Online]. Available: https://standards.ieee.org/wp-content/uploads/2022/03/IC22-003-Mobile-and-Transportable-Energy-Storage-Systems.pdf [Page 1.]

[6] L. Cheng, Y. Wan, Y. Zhou, and D. W. Gao, "Operational Reliability Modeling and Assessment of Battery Energy Storage Based on Lithium-ion Battery Lifetime Degradation," *Journal of Modern Power Systems and Clean Energy*, vol. 10, no. 6, pp. 1738–1749, Nov. 2022. doi: 10.35833/MPCE.2021.000197 Conference Name: Journal of Modern Power Systems and Clean Energy. [Pages 2, 6, 15, 20, 22, 24, and 41.]

[7] T. T. Pham, T. C. Kuo, D. M. Bui, D. P. Le, Q. A. Pham, and T. D. Nguyen, "Impact of Dynamic Operation on Reliability of an Aggregate Battery Energy Storage System," in *2019 IEEE PES Asia-Pacific Power and Energy Engineering Conference (APPEEC)*, Dec. 2019. doi: 10.1109/APPEEC45492.2019.8994553 pp. 1–6. [Pages 2 and 15.]

[8] T. Jin, P. Wang, and Q. Huang, "A Practical MTBF Estimate for PCB Design Considering Component and Non-Component Failures," in *RAMS '06. Annual Reliability and Maintainability Symposium, 2006.*, Jan. 2006. doi: 10.1109/RAMS.2006.1677440 pp. 604–610, iSSN: 0149-144X. [Pages 2 and 24.]

[9] B. Zakeri and S. Syri, "Electrical Energy Storage Systems: A Comparative Life Cycle Cost Analysis," *Renewable and Sustainable Energy Reviews*, vol. 42, pp. 569–596, Feb. 2015. doi: 10.1016/j.rser.2014.10.011. [Online]. Available: https://www.sciencedirect.com/science/article/pii/S1364032114008284 [Pages xiii, 2, 37, 38, 56, and 57.]

[10] D. M. Davies, M. G. Verde, O. Mnyshenko, Y. R. Chen, R. Rajeev, Y. S. Meng, and G. Elliott, "Combined Economic and Technological Evaluation of Battery Energy Storage for Grid Applications," *Nature Energy*, vol. 4, no. 1, pp. 42–50, Jan. 2019. doi: 10.1038/s41560-018-0290-1 Number: 1 Publisher: Nature Publishing Group. [Online]. Available: https://www.nature.com/articles/s41560-018-0290-1 [Page 6.]

[11] E. Pusceddu, B. Zakeri, and G. Castagneto Gissey, "Synergies Between Energy Arbitrage and Fast Frequency Response for Battery Energy Storage Systems," *Applied Energy*, vol. 283, p. 116274, Feb. 2021. doi: 10.1016/j.apenergy.2020.116274. [Online]. Available: https:

//www.sciencedirect.com/science/article/pii/S0306261920316640 [Page 6.]

[12] Asian Development Bank, "Handbook on Battery Energy Storage System," Asian Development Bank, Manila, Philippines, Tech. Rep., Dec. 2018, edition: 0 ISBN: 9789292614713 9789292614706. [Online]. Available: https://www.adb.org/publications/battery-energy-storage-system-handbook [Pages 6, 7, 37, and 57.]

[13] Clean Energy Institute, "Lithium-Ion Battery." [Online]. Available: https://www.cei.washington.edu/education/science-of-solar/battery-technology/ [Page 7.]

[14] J. Liu, C. Hu, A. Kimber, and Z. Wang, "Uses, Cost-Benefit Analysis, and Markets of Energy Storage Systems for Electric Grid Applications," *Journal of Energy Storage*, vol. 32, p. 101731, Dec. 2020. doi: 10.1016/j.est.2020.101731. [Online]. Available: https://www.sciencedirect.com/science/article/pii/S2352152X20315681 [Pages 7, 37, and 60.]

[15] H. C. Hesse, M. Schimpe, D. Kucevic, and A. Jossen, "Lithium-Ion Battery Storage for the Grid—A Review of Stationary Battery Storage System Design Tailored for Applications in Modern Power Grids," *Energies*, vol. 10, no. 12, p. 2107, Dec. 2017. doi: 10.3390/en10122107 Number: 12 Publisher: Multidisciplinary Digital Publishing Institute. [Online]. Available: https://www.mdpi.com/1996-1073/10/12/2107 [Page 7.]

[16] T. Kousksou, P. Bruel, A. Jamil, T. El Rhafiki, and Y. Zeraouli, "Energy Storage: Applications and Challenges," *Solar Energy Materials and Solar Cells*, vol. 120, pp. 59–80, Jan. 2014. doi: 10.1016/j.solmat.2013.08.015. [Online]. Available: https://www.sciencedirect.com/science/article/pii/S0927024813004145 [Page 7.]

[17] C. Hendricks, N. Williard, S. Mathew, and M. Pecht, "A failure modes, mechanisms, and effects analysis (FMMEA) of lithium-ion batteries," *Journal of Power Sources*, vol. 297, pp. 113–120, Nov. 2015. doi: 10.1016/j.jpowsour.2015.07.100. [Online]. Available: https://www.sciencedirect.com/science/article/pii/S0378775315301233 [Pages xiii and 8.]

[18] H. Wang, M. Liserre, and F. Blaabjerg, "Toward Reliable Power Electronics: Challenges, Design Tools, and Opportunities," *IEEE Industrial Electronics Magazine*, vol. 7, no. 2, pp. 17–26, Jun. 2013. doi: 10.1109/MIE.2013.2252958 Conference Name: IEEE Industrial Electronics Magazine. [Page 7.]

[19] S. Peyghami, P. Palensky, and F. Blaabjerg, "An Overview on the Reliability of Modern Power Electronic Based Power Systems," *IEEE Open Journal of Power Electronics*, vol. 1, pp. 34–50, 2020. doi: 10.1109/OJPEL.2020.2973926 [Page 7.]

[20] A. Abuelnaga, M. Narimani, and A. S. Bahman, "A Review on IGBT Module Failure Modes and Lifetime Testing," *IEEE Access*, vol. 9, pp. 9643–9663, 2021. doi: 10.1109/ACCESS.2021.3049738 Conference Name: IEEE Access. [Page 7.]

[21] J. Falck, C. Felgemacher, A. Rojko, M. Liserre, and P. Zacharias, "Reliability of Power Electronic Systems: An Industry Perspective," *IEEE Industrial Electronics Magazine*, vol. 12, no. 2, pp. 24–35, Jun. 2018. doi: 10.1109/MIE.2018.2825481 Conference Name: IEEE Industrial Electronics Magazine. [Page 7.]

[22] G. Haines, "Basic Operation of a Battery Energy Storage System (BESS)," The University of Adelaide, Tech. Rep., 2018. [Online]. Available: https://www.adelaide.edu.au/energy-storage/docs/aeskb-case-study-1-basic-operation-of-a-bess.PDF [Page 7.]

[23] X. Jin, E. W. M. Ma, T. W. S. Chow, and M. Pecht, "An Investigation into Fan Reliability," in *Proceedings of the IEEE 2012 Prognostics and System Health Management Conference (PHM-2012 Beijing)*, May 2012. doi: 10.1109/PHM.2012.6228836 pp. 1–7, iSSN: 2166-5656. [Pages 7, 32, 33, and 41.]

[24] F. Sebaaly, H. Y. Kanaan, and N. Moubayed, "Three-Level Neutral-Point-Clamped Inverters in Transformerless Pv Systems — State of the Art," in *MELECON 2014 - 2014 17th IEEE Mediterranean Electrotechnical Conference*, Apr. 2014. doi: 10.1109/MELCON.2014.6820496 pp. 1–7, iSSN: 2158-8481. [Page 8.]

[25] M. Frisch, V. GmbH, B. Str, T. Ernö, and V. Kft, "Advantages of NPC Inverter Topologies with Power Modules," Vincotech Kft, Tech. Rep., Jul. 2009. [Online]. Available: https://www.vincotech.com/fileadmin/

user_upload/content_media/documents/pdf/support-documents/technical-papers/Vincotech_TP_2009-07-001-v01_Advantages_of_NPC_Inverter_Topologies_with_Power_Modules.pdf [Page 8.]

[26] Vincotech, "flowNPC 2 | Vincotech." [Online]. Available: https://www.vincotech.com/products/product-details/30-PT07NIB300S503-LH36F58Y.html [Pages xi and 9.]

[27] N. Hou, "Condition Based Reliability Evaluation and Maintenance Strategy for Battery Energy Storage System," Ph.D. dissertation, KTH Royal Institute of Technology, 2022. [Online]. Available: http://urn.kb.se/resolve?urn=urn:nbn:se:kth:diva-321823 [Pages xiii, 9, 13, and 34.]

[28] H. Wang and F. Blaabjerg, "Power Electronics Reliability: State of the Art and Outlook," *IEEE Journal of Emerging and Selected Topics in Power Electronics*, vol. 9, no. 6, pp. 6476–6493, Dec. 2021. doi: 10.1109/JESTPE.2020.3037161 Conference Name: IEEE Journal of Emerging and Selected Topics in Power Electronics. [Page 9.]

[29] A. Hanif, Y. Yu, D. DeVoto, and F. Khan, "A Comprehensive Review Toward the State-of-the-Art in Failure and Lifetime Predictions of Power Electronic Devices," *IEEE Transactions on Power Electronics*, vol. 34, no. 5, pp. 4729–4746, May 2019. doi: 10.1109/TPEL.2018.2860587 Conference Name: IEEE Transactions on Power Electronics. [Page 9.]

[30] M. Ciappa, "Selected Failure Mechanisms of Modern Power Modules," *Microelectronics Reliability*, vol. 42, no. 4, pp. 653–667, Apr. 2002. doi: 10.1016/S0026-2714(02)00042-2. [Online]. Available: https://www.sciencedirect.com/science/article/pii/S0026271402000422 [Page 9.]

[31] C. Papadopoulos, C. Corvasce, A. Kopta, D. Schneider, G. Pâques, and M. Rahimo, "The Influence of Humidity on the High Voltage Blocking Reliability of Power IGBT Modules and Means of Protection," *Microelectronics Reliability*, vol. 88-90, pp. 470–475, Sep. 2018. doi: 10.1016/j.microrel.2018.07.130. [Online]. Available: https://www.sciencedirect.com/science/article/pii/S0026271418307108 [Page 9.]

[32] Fronius, "Active Cooling Technology." [Online]. Available: https://www.fronius.com/en/solar-energy/installers-partners/products-solutions/features/active-cooling-technology [Pages 9 and 43.]

[33] H. Huang and P. A. Mawby, "A Lifetime Estimation Technique for Voltage Source Inverters," *IEEE Transactions on Power Electronics*, vol. 28, no. 8, pp. 4113–4119, Aug. 2013. doi: 10.1109/TPEL.2012.2229472 Conference Name: IEEE Transactions on Power Electronics. [Page 9.]

[34] K. K. Pandey, M. Kumar, A. Kumari, and J. Kumar, "Bidirectional DC-DC Buck-Boost Converter for Battery Energy Storage System and PV Panel," in *Modeling, Simulation and Optimization*, ser. Smart Innovation, Systems and Technologies, B. Das, R. Patgiri, S. Bandyopadhyay, and V. E. Balas, Eds. Singapore: Springer, 2021, pp. 681–693. ISBN 9789811598296. [Online]. Available: https://doi.org/10.1007/978-981-15-9829-6_54 [Page 9.]

[35] B. Yao, H. Chen, X.-Q. He, Q.-Z. Xiao, and X.-J. Kuang, "Reliability and Failure Analysis of DC/DC Converter and Case Studies," in *2013 International Conference on Quality, Reliability, Risk, Maintenance, and Safety Engineering (QR2MSE)*, Jul. 2013. doi: 10.1109/QR2MSE.2013.6625766 pp. 1133–1135. [Pages 9 and 10.]

[36] Vincotech, "flow3xBUCK-BOOST S3 | Vincotech." [Online]. Available: https://www.vincotech.com/products/product-details/B0-SP10NDA100S7-LU18F08T.html [Pages xi and 10.]

[37] F. Chen, R. Huang, C. Wang, X. Yu, H. Liu, Q. Wu, K. Qian, and R. Bhagat, "Air and PCM Cooling for Battery Thermal Management Considering Battery Cycle Life," *Applied Thermal Engineering*, vol. 173, p. 115154, Jun. 2020. doi: 10.1016/j.applthermaleng.2020.115154. [Online]. Available: https://www.sciencedirect.com/science/article/pii/S1359431119370176 [Pages 10, 21, and 44.]

[38] S. S. Madani, M. J. Swierczynski, and S. K. Kær, "A Review of Thermal Management and Safety for Lithium Ion Batteries," in *2017 Twelfth International Conference on Ecological Vehicles and Renewable Energies (EVER)*, Apr. 2017. doi: 10.1109/EVER.2017.7935914 pp. 1–20. [Pages xi, 10, 11, 36, and 44.]

[39] S. Chacko and S. Charmer, "Lithium-Ion Pack Thermal Modeling and Evaluation of Indirect Liquid Cooling for Electric Vehicle Battery Thermal Management," in *Innovations in Fuel Economy and Sustainable Road Transport*. Woodhead Publishing, Jan. 2011, pp. 13–21. ISBN 978-0-85709-213-7. [Online]. Available: https://www.sciencedirect.com/science/article/pii/B9780857092137500024 [Page 11.]

[40] M. Mousavi, S. Hoque, S. Rahnamayan, I. Dincer, and G. F. Naterer, "Optimal Design of an Air-Cooling System for a Li-Ion Battery Pack in Electric Vehicles with a Genetic Algorithm," in *2011 IEEE Congress of Evolutionary Computation (CEC)*, Jun. 2011. doi: 10.1109/CEC.2011.5949840 pp. 1848–1855, iSSN: 1941-0026. [Page 11.]

[41] J. Wang, J. Purewal, P. Liu, J. Hicks-Garner, S. Soukazian, E. Sherman, A. Sorenson, L. Vu, H. Tataria, and M. W. Verbrugge, "Degradation of Lithium Ion Batteries Employing Graphite Negatives and Nickel–Cobalt–Manganese Oxide + Spinel Manganese Oxide Positives: Part 1, Aging Mechanisms and Life Estimation," *Journal of Power Sources*, vol. 269, pp. 937–948, Dec. 2014. doi: 10.1016/j.jpowsour.2014.07.030. [Online]. Available: https://www.sciencedirect.com/science/article/pii/S037877531401074X [Page 11.]

[42] J. Neubauer and E. Wood, "Thru-Life Impacts of Driver Aggression, Climate, Cabin Thermal Management, and Battery Thermal Management on Battery Electric Vehicle Utility," *Journal of Power Sources*, vol. 259, pp. 262–275, Aug. 2014. doi: 10.1016/j.jpowsour.2014.02.083. [Online]. Available: https://www.sciencedirect.com/science/article/pii/S0378775314002766 [Page 11.]

[43] T. Yuksel, S. Litster, V. Viswanathan, and J. J. Michalek, "Plug-in Hybrid Electric Vehicle LifePO4 Battery Life Implications of Thermal Management, Driving Conditions, and Regional Climate," *Journal of Power Sources*, vol. 338, pp. 49–64, Jan. 2017. doi: 10.1016/j.jpowsour.2016.10.104. [Online]. Available: https://www.sciencedirect.com/science/article/pii/S0378775316315130 [Page 11.]

[44] S. B. Rane, P. R. Potdar, and S. Rane, "Accelerated Life Testing for Reliability Improvement: A Case Study on Moulded Case Circuit Breaker (MCCB) Mechanism," *International Journal of System Assurance Engineering and Management*, vol. 10, no. 6, pp. 1668–1690, Dec. 2019. doi: 10.1007/s13198-019-00914-6. [Online]. Available: http://link.springer.com/10.1007/s13198-019-00914-6 [Pages 12 and 44.]

[45] G. Mathew and S. B. Rane, "Reliability Estimation of Molded Case Circuit Breaker in Development Phase," in *Proceedings of International Conference on Intelligent Manufacturing and Automation*, ser. Lecture Notes in Mechanical Engineering, H. Vasudevan, V. K. N. Kottur, and A. A. Raina, Eds. Singapore: Springer, 2020. doi: 10.1007/978-981-15-4485-9$_5$9.$ISBN9789811544859pp.581 - -589.[Page\ 12.]$

[46] C. Suwanasri, S. Lipirodjanapong, T. Suwanasri, and W. Wangdee, "Failure Rate Analysis of Circuit Breaker and its Preventive Maintenance Application," in *2014 International Conference on Probabilistic Methods Applied to Power Systems (PMAPS)*, Jul. 2014. doi: 10.1109/PMAPS.2014.6960623 pp. 1–6. [Page 12.]

[47] K. Jeong, Y. Kim, C. Kim, and O. Kwon, "A Study on the Statistical Life Span Estimation of Aged Low-Voltage Circuit Breakers," *Journal of Electrical Engineering & Technology*, vol. 15, no. 6, pp. 2833–2839, Nov. 2020. doi: 10.1007/s42835-020-00546-y. [Online]. Available: https://doi.org/10.1007/s42835-020-00546-y [Page 12.]

[48] M. Babb and A. Trusty, "A Balanced Approach to Molded Case Circuit Breaker Maintenance," in *2019 IEEE IAS Electrical Safety Workshop (ESW)*, Mar. 2019. doi: 10.1109/ESW41045.2019.9024751 pp. 1–7, iSSN: 2326-330X. [Page 12.]

[49] S. Liu, Y. Yang, H. Wang, Z. Wang, Z. Liu, Y. Geng, and J. Wang, "Dc Current Interruption by a Combination of Electric Fuse and Vacuum Switch," in *2015 3rd International Conference on Electric Power Equipment – Switching Technology (ICEPE-ST)*, Oct. 2015. doi: 10.1109/ICEPE-ST.2015.7368336 pp. 246–250. [Page 12.]

[50] C. Gera and S. Sharma, "A Method to Diagnose Failures in High Voltage Contactors and Fuse for Safe Operation of Battery Pack," in *2019 IEEE Transportation Electrification Conference (ITEC-India)*, Dec. 2019. doi: 10.1109/ITEC-India48457.2019.ITECINDIA2019-105 pp. 1–4. [Page 12.]

[51] Y. Chu, Z. Li, K. Wang, H. Xu, X. Guo, and N. Su, "Analysis and Design of 24V DC Control Contactor," in *The 16th IET International Conference on AC and DC Power Transmission (ACDC 2020)*, vol. 2020, Jul. 2020. doi: 10.1049/icp.2020.0025 pp. 2006–2010. [Page 12.]

[52] M. J. Heathcote, "1 - Transformer Theory," in *J & P Transformer Book (Thirteenth Editon)*, M. J. Heathcote, Ed. Oxford: Newnes, Jan. 2007, pp. 1–13. ISBN 978-0-7506-8164-3. [Online]. Available: https://www.sciencedirect.com/science/article/pii/B978075068164350003X [Page 13.]

[53] S. Mishra, A. Baral, and S. Chakravorti, "Assessing the condition of Nomex paper-based Insulation in Open Wound and VPI type Dry-type Transformer using Frequency Domain Spectroscopy Data," in *2020 International Conference for Emerging Technology (INCET)*, Jun. 2020. doi: 10.1109/INCET49848.2020.9154144 pp. 1–5. [Page 13.]

[54] P. Chen, Y. Huang, F. Zeng, Y. Jin, X. Zhao, and J. Wang, "Review on Insulation and Reliability of Dry-Type Transformer," in *2019 IEEE Sustainable Power and Energy Conference (iSPEC)*, Nov. 2019. doi: 10.1109/iSPEC48194.2019.8975106 pp. 398–402. [Page 13.]

[55] P. E. Blanco Alonso, A. Meana-Fernández, and J. M. Fernández Oro, "Thermal Response and Failure Mode Evaluation of a Dry-Type Transformer," *Applied Thermal Engineering*, vol. 120, pp. 763–771, Jun. 2017. doi: 10.1016/j.applthermaleng.2017.04.007. [Online]. Available: https://www.sciencedirect.com/science/article/pii/S1359431116331210 [Pages 13 and 48.]

[56] J. van Bolhuis, E. Gulski, and J. Smit, "Monitoring and Diagnostic of Transformer Solid Insulation," *IEEE Transactions on Power Delivery*, vol. 17, no. 2, pp. 528–536, Apr. 2002. doi: 10.1109/61.997930 Conference Name: IEEE Transactions on Power Delivery. [Page 13.]

[57] M. Utakrue and K. Hongesombut, "Impact Analysis of Electric Vehicle Quick Charging to Power Transformer Life Time in Distribution System," in *2018 IEEE Transportation Electrification Conference and Expo, Asia-Pacific (ITEC Asia-Pacific)*, Jun. 2018. doi: 10.1109/ITEC-AP.2018.8433281 pp. 1–5. [Pages 13 and 48.]

[58] K. Najdenkoski, G. Rafajlovski, and V. Dimcev, "Thermal Aging of Distribution Transformers According to IEEE and IEC Standards," in

2007 IEEE Power Engineering Society General Meeting, Jun. 2007. doi: 10.1109/PES.2007.385642 pp. 1–5, iSSN: 1932-5517. [Pages 13 and 48.]

[59] C. W. T. McLyman, *Transformer and Inductor Design Handbook, Third Edition*, 3rd ed. Boca Raton: CRC Press, Mar. 2004. ISBN 978-0-429-22398-3 [Pages 13 and 48.]

[60] The Institute of Electrical and Electronics Engineers, Inc., "IEEE Guide for Loading Dry-Type Distribution and Power Transformers," *ANSI/IEEE Std C57.96-1989*, pp. 0_1–, 1989. doi: 10.1109/IEEESTD.1989.95396 Conference Name: ANSI/IEEE Std C57.96-1989. [Pages 13, 47, and 48.]

[61] A. Franzén and S. Karlsson, "Failure Modes and Effects Analysis of Transformers," KTH Royal Institute of Technology, Sweden, Tech. Rep., 2007. [Online]. Available: http://www.generalpurposehosting.com/updates/TRITA-EE_2007_040.pdf [Pages xiii and 13.]

[62] B. Huang, H. Zhang, and M. Lu, "Software FMEAApproach Based on Failure Modes Database," in *2009 8th International Conference on Reliability, Maintainability and Safety*, Jul. 2009. doi: 10.1109/ICRMS.2009.5270088 pp. 749–753. [Pages xiii and 14.]

[63] G. K. Morris, D. D. Yellamati, and M. A. Cymerman, "Predicting Circuit Board Reliability for Motor Drives Under Varying Application and Environmental Conditions," in *2014 Reliability and Maintainability Symposium*, Jan. 2014. doi: 10.1109/RAMS.2014.6798511 pp. 1–6, iSSN: 0149-144X. [Pages 14 and 15.]

[64] X. Shu, W. Yang, Y. Guo, K. Wei, B. Qin, and G. Zhu, "A Reliability Study of Electric Vehicle Battery from the Perspective of Power Supply System," *Journal of Power Sources*, vol. 451, p. 227805, Mar. 2020. doi: 10.1016/j.jpowsour.2020.227805. [Online]. Available: https://www.sciencedirect.com/science/article/pii/S0378775320301087 [Pages xiii, xiv, 15, 35, 36, 49, 63, 86, and 87.]

[65] Naval Surface Warfare Center, "Handbook of Reliability Prediction Procedures for Mechanical Equipment," United States Navy, Research and Development Report, May 1992, section: Technical Reports. [Online]. Available: https://apps.dtic.mil/sti/citations/ADA273174 [Pages 15 and 36.]

[66] IEC, "IEC TR 62380: Reliability Date Handbook-Universal Model for Reliability Prediction of Electronics-components, PCBs and equipment, NEQ)," Geneva, 2004, iEC TR 62380. [Page 15.]

[67] American Department of Defense, *Military Handbook : Reliability Prediction of Electronic Equipment*. Washington DC: Department of Defense Washington DC, Dec. 1991. [Pages 15, 35, and 36.]

[68] A. Manenti, A. Abba, A. Merati, S. M. Savaresi, and A. Geraci, "A New BMS Architecture Based on Cell Redundancy," *IEEE Transactions on Industrial Electronics*, vol. 58, no. 9, pp. 4314–4322, Sep. 2011. doi: 10.1109/TIE.2010.2095398 Conference Name: IEEE Transactions on Industrial Electronics. [Page 15.]

[69] S. Ebbesen, P. Elbert, and L. Guzzella, "Battery State-of-Health Perceptive Energy Management for Hybrid Electric Vehicles," *IEEE Transactions on Vehicular Technology*, vol. 61, no. 7, pp. 2893–2900, Sep. 2012. doi: 10.1109/TVT.2012.2203836 Conference Name: IEEE Transactions on Vehicular Technology. [Pages xiii, 15, 16, 20, 21, and 42.]

[70] Q. Xia, Z. Wang, Y. Ren, B. Sun, D. Yang, and Q. Feng, "A Reliability Design Method for a Lithium-Ion Battery Pack Considering the Thermal Disequilibrium in Electric Vehicles," *Journal of Power Sources*, vol. 386, pp. 10–20, May 2018. doi: 10.1016/j.jpowsour.2018.03.036. [Online]. Available: https://www.sciencedirect.com/science/article/pii/S037877531830260X [Pages 15, 16, 22, and 24.]

[71] Z. Liu, C. Tan, and F. Leng, "A Reliability-Based Design Concept for Lithium-Ion Battery Pack in Electric Vehicles," *Reliability Engineering & System Safety*, vol. 134, pp. 169–177, Feb. 2015. doi: 10.1016/j.ress.2014.10.010. [Online]. Available: https://www.sciencedirect.com/science/article/pii/S0951832014002506 [Pages 15, 16, 22, and 41.]

[72] Y. Chen, Y. Zheng, F. Luo, J. Wen, and Z. Xu, "Reliability Evaluation of Distribution Systems with Mobile Energy Storage Systems," *IET Renewable Power Generation*, vol. 10, no. 10, pp. 1562–1569, 2016. doi: 10.1049/iet-rpg.2015.0608 _eprint: https://onlinelibrary.wiley.com/doi/pdf/10.1049/iet-rpg.2015.0608. [Online]. Available: https://onlinelibrary.wiley.com/doi/abs/10.1049/iet-rpg.2015.0608 [Page 15.]

[73] M. Liu, W. Li, C. Wang, R. Billinton, and J. Yu, "Reliability Evaluation of a Tidal Power Generation System Considering Tidal Current Speeds," *IEEE Transactions on Power Systems*, vol. 31, no. 4, pp. 3179–3188, Jul. 2016. doi: 10.1109/TPWRS.2015.2473797 Conference Name: IEEE Transactions on Power Systems. [Pages 16, 25, and 31.]

[74] H. Liu and M. Panteli, "A Reliability Analysis and Comparison of Battery Energy Storage Systems," in *2019 IEEE PES Innovative Smart Grid Technologies Europe (ISGT-Europe)*, Sep. 2019. doi: 10.1109/ISGTEurope.2019.8905658 pp. 1–5. [Pages 16, 20, and 21.]

[75] Endrenyi, John and others, *Reliability Modeling in Electric Power Systems*. Wiley New York, 1978. ISBN 0471996645 [Page 17.]

[76] P. Hilber, "Component Reliability Importance Indices for Maintenance Optimization of Electrical Networks," Licentiate Thesis, KTH Royal Institute of Technology, 2005. [Online]. Available: http://www.diva-portal.org/smash/get/diva2:8450/FULLTEXT01.pdf [Pages 17, 18, 38, and 39.]

[77] Mohammad Modarres, Mark P. Kaminskiy, and Vasiliy Krivtsov, *Reliability Engineering and Risk Analysis*, 3rd ed. Boca Raton: CRC Press, Nov. 2016. ISBN 978-1-315-38242-5. [Online]. Available: https://doi-org.focus.lib.kth.se/10.1201/9781315382425 [Pages xi, 17, 18, 19, 20, and 34.]

[78] J. Carl Wallnerström and P. Hilber, *Reliability Analysis and Asset Management Applied to Power Distribution*. KTH Royal Institute of Technology, 2014. ISBN 978-91-637-5385-5 [Page 19.]

[79] J. Wang, P. Liu, J. Hicks-Garner, E. Sherman, S. Soukiazian, M. Verbrugge, H. Tataria, J. Musser, and P. Finamore, "Cycle-Life Model for Graphite-LiFePO4 Cells," *Journal of Power Sources*, vol. 196, no. 8, pp. 3942–3948, Apr. 2011. doi: 10.1016/j.jpowsour.2010.11.134. [Online]. Available: https://www.sciencedirect.com/science/article/pii/S0378775310021269 [Pages xiii, 20, and 21.]

[80] D. U. Sauer and H. Wenzl, "Comparison of Different Approaches for Lifetime Prediction of Electrochemical Systems—Using Lead-Acid Batteries as Example," *Journal of Power Sources*, vol. 176, no. 2, pp. 534–546, Feb. 2008. doi: 10.1016/j.jpowsour.2007.08.057. [Online]. Available: https://www.sciencedirect.com/science/article/pii/S0378775307016199 [Page 20.]

[81] R. Tolomeo, G. De Feo, R. Adami, and L. Sesti Osséo, "Application of Life Cycle Assessment to Lithium Ion Batteries in the Automotive Sector," *Sustainability*, vol. 12, no. 11, p. 4628, Jan. 2020. doi: 10.3390/su12114628 Number: 11 Publisher: Multidisciplinary Digital Publishing Institute. [Online]. Available: https://www.mdpi.com/2071-1050/12/11/4628 [Page 20.]

[82] F. Arshad, J. Lin, N. Manurkar, E. Fan, A. Ahmad, M.-u.-N. Tariq, F. Wu, R. Chen, and L. Li, "Life Cycle Assessment of Lithium-Ion Batteries: A Critical Review," *Resources, Conservation and Recycling*, vol. 180, p. 106164, May 2022. doi: 10.1016/j.resconrec.2022.106164. [Online]. Available: https://www.sciencedirect.com/science/article/pii/S092134492200012X [Page 20.]

[83] L. gregory, *The Universal Generating Function in Reliability Analysis and Optimization*, ser. Springer Series in Reliability Engineering. London: Springer-Verlag, 2005. ISBN 978-1-85233-927-2. [Online]. Available: http://link.springer.com/10.1007/1-84628-245-4 [Page 22.]

[84] G. Levitin, A. Lisnianski, H. Haim, and D. Elmakis, "Genetic Algorithm and Universal Generating Function Technique for Solving Problems of Power System Reliability Optimization," in *DRPT2000. International Conference on Electric Utility Deregulation and Restructuring and Power Technologies. Proceedings (Cat. No.00EX382)*, Apr. 2000. doi: 10.1109/DRPT.2000.855730 pp. 582–586. [Page 22.]

[85] J. Marin and R. Pollard, "Experience Report on the FIDES Reliability Prediction Method," in *Annual Reliability and Maintainability Symposium, 2005. Proceedings.*, Jan. 2005. doi: 10.1109/RAMS.2005.1408330 pp. 8–13, iSSN: 0149-144X. [Page 24.]

[86] D. Nicholls, "What is 217Plus/sup TM/ and Where Did It Come From?" in *2007 Annual Reliability and Maintainability Symposium*, Jan. 2007. doi: 10.1109/RAMS.2007.328101 pp. 22–27, iSSN: 0149-144X. [Page 24.]

[87] Q. S. Incorporated (U.S.), W. Denson, P. Lein, and D. Nicholls, *Handbook of 217Plus Reliability Prediction Models*. Quanterion Solutions Incorporated, 2015. ISBN 978-1-933904-95-5. [Online]. Available: https://books.google.se/books?id=hcxLrgEACAAJ [Pages xiii, 24, 25, 26, 27, 28, 29, 30, 35, 36, 41, 49, 84, and 85.]

[88] S. Danfoss, "3L NPC & TNPC Topology Application Note." [Online]. Available: https://www.semikron-danfoss.com/dl/service-support/downloads/download/semikron-application-note-3l-npc-tnpc-topology-en-2015-10-12-rev-05.pdf [Pages 30 and 31.]

[89] B. Schroeder and G. A. Gibson, "Disk Failures in the Real World: What Does an MTTF of 1,000,000 Hours Mean to You?" in *FAST'07*, San Jose, CA, 2007.

[Online]. Available: https://www.cs.toronto.edu/~bianca/papers/fast07.pdf [Page 32.]

[90] IPC, "IPC-9591: Performance Parameters (Mechanical, Electrical, Environmental and Quality/Reliability) for Air Moving Device." Illinois, 2006. [Online]. Available: https://www.ipc.org/TOC/IPC-9591.pdf [Page 33.]

[91] T. T. Pham, T. C. Kuo, D. M. Bui, M. T. Cao, T. P. Nguyen, and T. D. Nguyen, "Reliability Evaluation of an Aggregate Battery Energy Storage System Under Dynamic Operation," in *2020 IEEE International Conference on Power Electronics, Smart Grid and Renewable Energy (PESGRE2020)*, Jan. 2020. doi: 10.1109/PESGRE45664.2020.9070561 pp. 1–8. [Page 33.]

[92] International Electrotechnical Commission, IEC, "Iec 62061: Safety of Machinery – Functional Safety of Safety-Related Electrical, Electronic and Programmable Electronic Control Systems," Jun. 2005. [Page 34.]

[93] Siemens, "Safety Characteristics - Standard B10 Values/Failure Rates of Electromechanical S... - ID: 109739348 - Industry Support Siemens," 2022. [Online]. Available: https://support.industry.siemens.com/cs/document/109739348/safety-characteristics-standard-b10-values-failure-rates-of-electromechanical-sirius-and-sentron-products-?dti=0&dl=en&lc=de-DE [Pages 34 and 44.]

[94] G. Xu, X. Du, Z. Li, X. Zhang, M. Zheng, Y. Miao, Y. Gao, and Q. Liu, "Reliability Design of Battery Management System for Power Battery," *Microelectronics Reliability*, vol. 88-90, pp. 1286–1292, Sep. 2018. doi: 10.1016/j.microrel.2018.06.115. [Online]. Available: https://www.sciencedirect.com/science/article/pii/S0026271418305390 [Page 35.]

[95] A. A. H. Akinlabi and D. Solyali, "Configuration, Design, and Optimization of Air-Cooled Battery Thermal Management System for Electric Vehicles: A Review," *Renewable and Sustainable Energy Reviews*, vol. 125, p. 109815, Jun. 2020. doi: 10.1016/j.rser.2020.109815. [Online]. Available: https://www.sciencedirect.com/science/article/pii/S1364032120301106 [Page 36.]

[96] G. Zhao, X. Wang, M. Negnevitsky, and H. Zhang, "A Review of Air-Cooling Battery Thermal Management Systems for Electric and Hybrid Electric Vehicles," *Journal of Power Sources*, vol. 501, p. 230001, Jul. 2021. doi: 10.1016/j.jpowsour.2021.230001. [Online]. Available: https:

//www.sciencedirect.com/science/article/pii/S0378775321005292 [Pages 36 and 41.]

[97] K. Bradbury, L. Pratson, and D. Patiño-Echeverri, "Economic Viability of Energy Storage Systems Based on Price Arbitrage Potential in Real-Time U.S. Electricity Markets," *Applied Energy*, vol. 114, pp. 512–519, Feb. 2014. doi: 10.1016/j.apenergy.2013.10.010. [Online]. Available: https://www.sciencedirect.com/science/article/pii/S0306261913008301 [Page 37.]

[98] S. M. Schoenung, "Characteristics and Technologies for Long- vs. Short-Term Energy Storage: A Study by the DOE Energy Storage Systems Program," Sandia National Lab. (SNL-NM), Albuquerque, NM (United States); Sandia National Lab. (SNL-CA), Livermore, CA (United States), Tech. Rep. SAND2001-0765, Mar. 2001. [Online]. Available: https://www.osti.gov/biblio/780306 [Page 37.]

[99] ——, "Energy Storage Systems Cost Update: A Study for the DOE Energy Storage Systems Program." Sandia National Laboratories (SNL), Albuquerque, NM, and Livermore, CA (United States), Tech. Rep. SAND2011-2730, Apr. 2011. [Online]. Available: https://www.osti.gov/biblio/1013227 [Pages xiii and 38.]

[100] X. Tian, "Cooling Fan Reliability: Failure Criteria, Accelerated Life Testing, Modeling and Qualification," in *RAMS '06. Annual Reliability and Maintainability Symposium, 2006.*, Jan. 2006. doi: 10.1109/RAMS.2006.1677404 pp. 380–384, iSSN: 0149-144X. [Page 41.]

[101] A. Webber, "Calculating Useful Lifetimes of Embedded Processors," Texas Instruments, Application Report, 2014. [Online]. Available: https://www.ti.com/lit/an/sprabx4b/sprabx4b.pdf?ts=1683634649725 [Page 43.]

[102] D. J. Navamani, J. M. Sathik, A. Lavanya, D. Almakhles, Z. M. Ali, and S. H. E. A. Aleem, "Reliability Prediction and Assessment Models for Power Components: A Comparative Analysis," *Archives of Computational Methods in Engineering*, vol. 30, no. 1, pp. 497–520, Jan. 2023. doi: 10.1007/s11831-022-09806-8. [Online]. Available: https://doi.org/10.1007/s11831-022-09806-8 [Page 43.]

[103] L. Fischer, E. Mura, G. Qiao, P. O'Neill, S. von Arx, Q. Li, and Y. Ding, "HVDC Converter Cooling System with a Phase Change Dispersion," *Fluids*, vol. 6, no. 3, p. 117, Mar. 2021. doi: 10.3390/fluids6030117 Number: 3

Publisher: Multidisciplinary Digital Publishing Institute. [Online]. Available: https://www.mdpi.com/2311-5521/6/3/117 [Page 43.]

[104] IEEE, "IEEE Standard for General Requirements for Dry-Type Distribution and Power Transformers," *IEEE Std C57.12.01-2020 (Revision of IEEE Std C57.12.01-2015)*, pp. 1–49, Nov. 2020. doi: 10.1109/IEEESTD.2020.9269795 Conference Name: IEEE Std C57.12.01-2020 (Revision of IEEE Std C57.12.01-2015). [Page 46.]

[105] ——, "IEEE Guide for Determination of Hottest-Spot Temperature in Dry-Type Transformers," *IEEE Std C57.134-2013 (Revision of IEEE Std C57.134-2000)*, pp. 1–25, Jan. 2014. doi: 10.1109/IEEESTD.2014.6712026 Conference Name: IEEE Std C57.134-2013 (Revision of IEEE Std C57.134-2000). [Page 47.]

[106] J. D. Salciccioli, Y. Crutain, M. Komorowski, and D. C. Marshall, "Sensitivity Analysis and Model Validation," in *Secondary Analysis of Electronic Health Records*, MIT Critical Data, Ed. Cham: Springer International Publishing, 2016, pp. 263–271. ISBN 978-3-319-43742-2. [Online]. Available: https://doi.org/10.1007/978-3-319-43742-2_17 [Page 51.]

[107] A. G. Olabi, H. M. Maghrabie, O. H. K. Adhari, E. T. Sayed, B. A. A. Yousef, T. Salameh, M. Kamil, and M. A. Abdelkareem, "Battery Thermal Management Systems: Recent Progress and Challenges," *International Journal of Thermofluids*, vol. 15, p. 100171, Aug. 2022. doi: 10.1016/j.ijft.2022.100171. [Online]. Available: https://www.sciencedirect.com/science/article/pii/S2666202722000350 [Page 51.]

[108] W. Kuo and V. Prasad, "An Annotated Overview of System-Reliability Optimization," *IEEE Transactions on Reliability*, vol. 49, no. 2, pp. 176–187, Jun. 2000. doi: 10.1109/24.877336 Conference Name: IEEE Transactions on Reliability. [Page 54.]

[109] M. Abouei Ardakan, A. Zeinal Hamadani, and M. Alinaghian, "Optimizing Bi-Objective Redundancy Allocation Problem with a Mixed Redundancy Strategy," *ISA Transactions*, vol. 55, pp. 116–128, Mar. 2015. doi: 10.1016/j.isatra.2014.10.002. [Online]. Available: https://www.sciencedirect.com/science/article/pii/S0019057814002511 [Page 54.]

[110] T.-J. Hsieh, "Component Mixing with a Cold Standby Strategy for the Redundancy Allocation Problem," *Reliability Engineering & System Safety*, vol. 206, p. 107290, Feb. 2021. doi: 10.1016/j.ress.2020.107290. [Online]. Available: https://www.sciencedirect.com/science/article/pii/S0951832020307869 [Page 54.]

[111] M. Abouei Ardakan and A. Zeinal Hamadani, "Reliability–Redundancy Allocation Problem with Cold-Standby Redundancy Strategy," *Simulation Modelling Practice and Theory*, vol. 42, pp. 107–118, Mar. 2014. doi: 10.1016/j.simpat.2013.12.013. [Online]. Available: https://www.sciencedirect.com/science/article/pii/S1569190X13001937 [Page 54.]

[112] W. Bank, "Economic Analysis of Battery Energy Storage Systems," World Bank, Tech. Rep., May 2020, publisher: World Bank, Washington, DC. [Online]. Available: http://hdl.handle.net/10986/33971 [Page 55.]

[113] IEA, "Average Pack Price of Lithium-Ion Batteries and Share of Cathode Material Cost, 2011-2021 – Charts – Data & Statistics," 2022. [Online]. Available: https://www.iea.org/data-and-statistics/charts/average-pack-price-of-lithium-ion-batteries-and-share-of-cathode-material-cost-2011-2021 [Page 55.]

[114] L. Lander, E. Kallitsis, A. Hales, J. S. Edge, A. Korre, and G. Offer, "Cost and Carbon Footprint Reduction of Electric Vehicle Lithium-Ion Batteries Through Efficient Thermal Management," *Applied Energy*, vol. 289, p. 116737, May 2021. doi: 10.1016/j.apenergy.2021.116737. [Online]. Available: https://www.sciencedirect.com/science/article/pii/S0306261921002518 [Page 55.]

[115] S. M. Schoenung and W. V. Hassenzahl, "Long- Vs. Short-Term Energy Storage Technologies Analysis: A Life-Cycle Cost Study: A Study for the DOE Energy Storage Systems Program." Sandia National Laboratories (SNL), Albuquerque, NM, and Livermore, CA (United States), Tech. Rep. SAND2003-2783, Aug. 2003. [Online]. Available: https://www.osti.gov/biblio/918358 [Page 56.]

[116] M. C. C. Lima, L. P. Pontes, A. S. M. Vasconcelos, W. de Araujo Silva Junior, and K. Wu, "Economic Aspects for Recycling of Used Lithium-Ion Batteries from Electric Vehicles," *Energies*, vol. 15, no. 6, p. 2203, Jan. 2022. doi: 10.3390/en15062203 Number: 6 Publisher: Multidisciplinary Digital Publishing Institute. [Online]. Available: https://www.mdpi.com/1996-1073/15/6/2203 [Page 57.]

[117] National Renewable Energy Laboratory, "_GBResidential Battery Storage," 2021. [Online]. Available: atb.nrel.gov [Page 58.]

Appendix A

Parameters Values in the Reliability Estimations

A.1 RIAC Parameter Values

The parameters used in the reliability modelling for different power electronics components from RIAC 217™ is given in Table A.1.

Parameters	IGBT	Capacitor	Diodes	Transformer
λ_{OB}	0.000235	0.000634	0.001603	0.0001214
λ_{EB}	0.0001657	0.000351	0.002748	0.0001499
λ_{TCB}	0.00016	0.000083	0.02603	0.0000518
λ_{IND}	0.008899	0.000259	0.01158	0.0000386
λ_{SJB}	0.0015	0.00095	0.00021	-
β	0.281	0.033	0.223	0
DC_{1op}	0.23	0.17	0.23	0.38
Ea_{op}	0.2	0.3	0.3	0.24
$T_{Rdefault}$	60	0	60	10
$V_{sdefault}$	0.5	0	0.29	-
DC_{1nonop}	0.77	0.83	0.77	0.62
Ea_{nonop}	0.3	0.3	0.4	0.240
CR_1	754.38	1140.35	736.84	312
DT_1	80	21	80	21.94
n	-	17	-	-
C_1	-	0.1	-	-
S_1	-	0.6	-	-
CE	-	0.09	-	-

Table A.1: Power electronics parameters from RIAC 217plus™ [87]

The RIAC 217™ parameters for software reliability estimation are given in Table A.2.

SEI's CMM Level	Initial Design FD	DSL
5	0.5	0.01
4	1.0	0.03
3	2.0	0.05
2	3.0	0.07
1	5.0	0.10
1	5.0	0.10
Unrated	6.0	Not Estimated

Table A.2: FD and DSL of software prediction model [87]

A.2 Power Electronics Components Parameters

The parameters used in the inverter reliability calculation are given in Table A.3.

Parameter	IGBT	Capacitor	Diodes
$U_{CE0/d0}$ [V]	1.43	-	1.92
$r_{CE/T}$ [Ω]	0	-	0
cos (φ)	1	-	1
E_{on} [J]	2.72×10^{-3}	-	-
E_{off} [J]	1.88×10^{-3}	-	-
E_{rec} [J]	-	-	1.923×10^{-3}
U_{ref} [V]	650	-	650
I_{ref} [A]	260	-	215
$U_{CE/rev-applied}$ [V]	350	-	350
$U_{CE/rev-rated}$ [V]	650	-	650
R_{TH} [K/kW]	0.33	-	0.33
R_{CH} [K/kW]	3.4	-	3.4
f_{sw} [Hz]	10^6	-	10^6
C [μF]	-	0.033	-
S_A	-	0.5385	-

Table A.3: Inverter components parameters

The individual component's parameters used in the DC/DC converter reliability estimation is given in Table A.4.

The components used, quantity (Qty), and individual failure rate (λ_i) of BMS master and slave controllers are given in Table A.5 and A.6, respectively. While the parameters for total BMS failure rate calculation is given in Table A.7.

Parameter	IGBT	Capacitor	Diodes
$U_{CE0/d0}$ [V]	1.67	-	1.92
$r_{CE/T}$ [Ω]	1.5	-	1.5
cos (φ)	1	-	1
E_{on} [J]	2.72×10^{-3}	-	-
E_{off} [J]	1.88×10^{-3}	-	-
E_{rec} [J]	-	-	1.1×10^{-3}
U_{ref} [V]	650	-	600
I_{ref} [A]	100	-	100
$U_{CE/rev-applied}$ [V]	600	-	600
$U_{CE/rev-rated}$ [V]	950	-	950
R_{TH} [K/kW]	0.895	-	0.895
R_{CH} [K/kW]	0.66	-	0.66
f_{sw} [Hz]	100 000	-	100 000
C [μF]	-	0.047	-
S_A	-	1.0833	-

Table A.4: DC/DC components parameters

Component	Package Type	Qty	λ_i [FPMH]
Ceramic capacitor	0603-C	206	0.00049
Capacitance X2	MPX-X2-GMF	2	0.00069
Diodes	SMA	10	0.04010
Integrated chip	TSSOP	2	0.08100
Inductance	MSS	3	0.07800
Optocoupler	SO-8	4	0.08800
Relay	HF46F	4	0.02500
MOSFET	SOT-223	8	0.07100
Resistance of direct plug	AXIAL	4	0.00685
Resistance of Surface mounted	0603-R	110	0.00320
Master chip	LQFP144	1	0.15000

Table A.5: BMS master controller components [64]

Component	Package Type	Qty	λ_i [FPMH]
Ceramic capacitor	1206-C/0603C	126	0.00049
Capacitance X2	MPX-X2-GMF	2	0.00069
Diodes	SMA	10	0.04010
Op-amp chip	TSSOP	4	0.08100
Inductance	MSS	3	0.07800
MOSFET	SOB	5	0.07100
Resistance of surface mounted	0603-R/2512/ 1206	120	0.00310
LTC6811	SSOP-48	4	0.10100
Relay	JQC-32F	2	0.02510
Communication chip	SOP14	1	0.05200

Table A.6: BMS slave controller components [64]

Name	Symbol	Value
PCB layer coefficient of master controller	π_{cA5}	1.4
PCB layer coefficient of slave controller	π_{cA9}	1.4
Track width factor of the master controller	π_{LA5}	2
Track width factor of the slave controller	π_{LA9}	2
Tracks number of master controller	N_{pA5}	415
Tracks number of slave controller	N_{pA9}	386
Number of SMCs on PCB of master controller	N_{SB7}	609
Number of SMCs on PCB of slave controller	N_{SB10}	463
Number of THCs on PCB of master controller	N_{fA5}	10
Number of THCs on PCB of slave controller	N_{fA9}	4
The surface area of PCB for master control	S_{A5}	142
Surface area of PCB for slave control	S_{A9}	124

Table A.7: BMS parameters for failure rate calculation [64]

Appendix B

Detailed Cost Analysis

B.1 LCC Analysis Details Calculation

Year $-y$	0	1	2	3	4	5
NPF(y)	1	0.926	0.857	0.794	0.735	0.681
AEP(y) **[kWh]**	0	186 880	180 651	174 421	168 192	161 963
Investment Cost [€]	98 175	0	0	0	0	0
O&M Cost [€]	0	2 502	2 502	2 502	2 502	2 502
Residual Value [€]	0	0	0	0	0	0
Disposal Cost [€]	0	0	0	0	0	0
Charging Cost [€]	0	9 344	9 033	8 721	8 410	8 098
Revenue [€]	0	-29 901	-28 904	-27 907	-26 911	-25 914
Total Cost [€]	98 175	-18 055	-17 370	-16 685	-15 999	-15 314
NPV(y) **[€]**	98 175	-16 718	-14 892	-13 245	-11 760	-10 423

Year $-y$	6	7	8	9	10
NPF(y)	0.630	0.583	0.540	0.500	0.463
AEP(y) **[kWh]**	155 733	149 504	143 275	137 045	130 816
Investment Cost [€]	0	0	0	0	0
O&M Cost [€]	2 502	2 502	2 502	2 502	2 502
Residual Value [€]	0	0	0	0	-4 000
Disposal Cost [€]	0	0	0	0	2 960
Charging Cost [€]	7 787	7 475	7 164	6 852	6 541
Revenue [€]	-24 917	-23 921	-22 924	-21 927	-20 931
Total Cost [€]	-14 629	-13 944	-13 259	-12 573	-12 928
NPV(y) **[€]**	-9 219	-8 136	-7 163	-6 290	-5 988
NPS [€]	-5 658				

Table B.1: Scenario 2 LCC analysis: redundancy on inverter system

Year$-y$	0	1	2	3	4	5	6	7
NPF(y)	1	0.926	0.857	0.794	0.735	0.681	0.630	0.583
AEP(y) **[kWh]**	0	186 880	182 567	178 255	173 942	169 630	165 317	161 004
Investment Cost [€]	130 344	0	0	0	0	0	0	0
O&M Cost [€]	0	2 375	2 375	2 375	2 375	2 375	2 375	2 375
Residual Value [€]	0	0	0	0	0	0	0	0
Disposal Cost [€]	0	0	0	0	0	0	0	0
Charging Cost [€]	0	9 344	9 128	8 913	8 697	8 481	8 266	8 050
Revenue [€]	0	-29 901	-29 211	-28 521	-27 831	-27 141	-26 451	-25 761
Total Cost [€]	130 344	-18 182	-17 707	-17 233	-16 759	-16 284	-15 810	-15 335
NPV(y) **[€]**	130 344	-16 835	-15 181	-13 680	-12 318	-11 083	-9 963	-8 948

Year$-y$	8	9	10	11	12	13	14
NPF(y)	0.540	0.500	0.463	0.429	0.397	0.368	0.340
AEP(y) **[kWh]**	156 692	152 379	148 066	143 754	139 441	135 129	130 816
Investment Cost [€]	0	0	0	0	0	0	0
O&M Cost [€]	2 375	2 375	2 375	2 375	2 375	2 375	2 375
Residual Value [€]	0	0	0	0	0	0	-4 000
Disposal Cost [€]	0	0	0	0	0	0	5 920
Charging Cost [€]	7 835	7 619	7 403	7 188	6 972	6 756	6 541
Revenue [€]	-25 071	-24 381	-23 691	-23 001	-22 311	-21 621	-20 931
Total Cost [€]	-14 861	-14 387	-13 912	-13 438	-12 964	-12 489	-10 095
NPV(y) **[€]**	-8 029	-7 197	-6 444	-5 763	-5 148	-4 592	-3 437
NPS [€]	20 665						

Table B.2: Scenario 3 LCC analysis: redundancy on battery packs

Year$-y$	0	1	2	3	4	5
NPF(y)	1	0.926	0.857	0.794	0.735	0.681
AEP(y) **[kWh]**	0	186 880	181 274	175 667	170 061	164 454
Investment Cost [€]	90 931	0	0	0	0	0
O&M Cost [€]	0	2 502	2 502	2 502	2 502	2 502
Residual Value [€]	0	0	0	0	0	0
Disposal Cost [€]	0	0	0	0	0	0
Charging Cost [€]	0	9 344	9 064	8 783	8 503	8 223
Revenue [€]	0	-29 901	-29 004	-28 107	-27 210	-26 313
Total Cost [€]	90 931	-18 055	-17 438	-16 822	-16 205	-15 588
NPV(y) **[€]**	90 931	-16 718	-14 951	-13 354	-11 911	-10 609

Year$-y$	6	7	8	9	10	11
NPF(y)	0.630	0.583	0.540	0.500	0.463	0.429
AEP(y) **[kWh]**	158 848	153 242	147 635	142 029	136 422	130 816
Investment Cost [€]	0	0	0	0	0	0
O&M Cost [€]	2 502	2 502	2 502	2 502	2 502	2 502
Residual Value [€]	0	0	0	0	0	-4 000
Disposal Cost [€]	0	0	0	0	0	2 960
Charging Cost [€]	7 942	7 662	7 382	7 101	6 821	6 541
Revenue [€]	-25 416	-24 519	-23 622	-22 725	-21 828	-20 931
Total Cost [€]	-14 972	-14 355	-13 738	-13 121	-12 505	-12 928
NPV(y) **[€]**	-9 435	-8 376	-7 422	-6 564	-5 792	-5 545
NPS [€]	-14 201					

Table B.3: Scenario 4 LCC analysis: redundancy on BTMS

Year$-y$	0	1	2	3	4
NPF(y)	1	0.926	0.857	0.794	0.735
AEP(y) **[kWh]**	0	186 880	179 872	172 864	165 856
Investment Cost [€]	91 593	0	0	0	0
O&M Cost [€]	0	2 600	2 600	2 600	2 600
Residual Value [€]	0	0	0	0	0
Disposal Cost [€]	0	0	0	0	0
Charging Cost [€]	0	9 344	8 994	8 643	8 293
Revenue [€]	0	-29 901	-28 780	-27 658	-26 537
Total Cost [€]	91 593	-17 956	-17 185	-16 415	-15 644
NPV(y) **[€]**	91 593	-16 626	-14 734	-13 030	-11 499

Year$-y$	5	6	7	8	9
NPF(y)	0.681	0.630	0.583	0.540	0.500
AEP(y) **[kWh]**	158 848	151 840	144 832	137 824	130 816
Investment Cost [€]	0	0	0	0	0
O&M Cost [€]	2 600	2 600	2 600	2 600	2 600
Residual Value [€]	0	0	0	0	-4 000
Disposal Cost [€]	0	0	0	0	2 960
Charging Cost [€]	7 942	7 592	7 242	6 891	6 541
Revenue [€]	-25 416	-24 294	-23 173	-22 052	-20 931
Total Cost [€]	-14 873	-14 102	-13 331	-12 560	-12 829
NPV(y) **[€]**	-10 122	-8 887	-7 779	-6 786	-6 418
NPS [€]	-4 287				

Table B.4: Scenario 5 LCC analysis: redundancy on transformer

Year$-y$	0	1	2	3	4
NPF(y)	1	0.926	0.857	0.794	0.735
AEP(y) **[kWh]**	0	186 880	179 872	172 864	165 856
Investment Cost [€]	85 486	0	0	0	0
O&M Cost [€]	0	2 568	2 568	2 568	2 568
Residual Value [€]	0	0	0	0	0
Disposal Cost [€]	0	0	0	0	0
Charging Cost [€]	0	9 344	8 994	8 643	8 293
Revenue [€]	0	-29 901	-28 780	-27 658	-26 537
Total Cost [€]	85 486	-17 989	-17 218	-16 448	-15 677
NPV(y) **[€]**	85 486	-16 657	-14 762	-13 057	-11 523

Year$-y$	5	6	7	8	9
NPF(y)	0.681	0.630	0.583	0.540	0.500
AEP(y) **[kWh]**	158 848	151 840	144 832	137 824	130 816
Investment Cost [€]	0	0	0	0	0
O&M Cost [€]	2 568	2 568	2 568	2 568	2 568
Residual Value [€]	0	0	0	0	-4 000
Disposal Cost [€]	0	0	0	0	2 960
Charging Cost [€]	7 942	7 592	7 242	6 891	6 541
Revenue [€]	-25 416	-24 294	-23 173	-22 052	-20 931
Total Cost [€]	-14 906	-14 135	-13 364	-12 593	-12 862
NPV(y) **[€]**	-10 145	-8 907	-7 798	-6 804	-6 434
NPS [€]	-10 600				

Table B.5: Scenario 6 LCC analysis: redundancy on DC/DC converter

Year$-y$	0	1	2	3	4
NPF(y)	1	0.926	0.857	0.794	0.735
AEP(y) **[kWh]**	0	186 880	179 872	172 864	165 856
Investment Cost [€]	87 802	0	0	0	0
O&M Cost [€]	0	2 568	2 568	2 568	2 568
Residual Value [€]	0	0	0	0	0
Disposal Cost [€]	0	0	0	0	0
Charging Cost [€]	0	9 344	8 994	8 643	8 293
Revenue [€]	0	-29 901	-28 780	-27 658	-26 537
Total Cost [€]	87 802	-17 989	-17 218	-16 448	-15 677
NPV(y) **[€]**	87 802	-16 657	-14 762	-13 057	-11 523

Year$-y$	5	6	7	8	9
NPF(y)	0.681	0.630	0.583	0.540	0.500
AEP(y) **[kWh]**	158 848	151 840	144 832	137 824	130 816
Investment Cost [€]	0	0	0	0	0
O&M Cost [€]	2 568	2 568	2 568	2 568	2 568
Residual Value [€]	0	0	0	0	-4 000
Disposal Cost [€]	0	0	0	0	2 960
Charging Cost [€]	7 942	7 592	7 242	6 891	6 541
Revenue [€]	-25 416	-24 294	-23 173	-22 052	-20 931
Total Cost [€]	-14 906	-14 135	-13 364	-12 593	-12 862
NPV(y) **[€]**	-10 145	-8 907	-7 798	-6 804	-6 434
NPS [€]	-8 283				

Table B.6: Scenario 7 LCC analysis: redundancy on MCCB

Year$-y$	0	1	2	3	4
NPF(y)	1	0.926	0.857	0.794	0.735
AEP(y) **[kWh]**	0	186 880	179 872	172 864	165 856
Investment Cost [€]	86 422	0	0	0	0
O&M Cost [€]	0	2 600	2 600	2 600	2 600
Residual Value [€]	0	0	0	0	0
Disposal Cost [€]	0	0	0	0	0
Charging Cost [€]	0	9 344	8 994	8 643	8 293
Revenue [€]	0	-29 901	-28 780	-27 658	-26 537
Total Cost [€]	86 422	-17 956	-17 185	-16 415	-15 644
NPV(y) **[€]**	86 422	-16 626	-14 734	-13 030	-11 499

Year$-y$	5	6	7	8	9
NPF(y)	0.681	0.630	0.583	0.540	0.500
AEP(y) **[kWh]**	158 848	151 840	144 832	137 824	130 816
Investment Cost [€]	0	0	0	0	0
O&M Cost [€]	2 600	2 600	2 600	2 600	2 600
Residual Value [€]	0	0	0	0	-4 000
Disposal Cost [€]	0	0	0	0	2 960
Charging Cost [€]	7 942	7 592	7 242	6 891	6 541
Revenue [€]	-25 416	-24 294	-23 173	-22 052	-20 931
Total Cost [€]	-14 873	-14 102	-13 331	-12 560	-12 829
NPV(y) **[€]**	-10 122	-8 887	-7 779	-6 786	-6 418
NPS [€]	-9 458				

Table B.7: Scenario 8 LCC analysis: redundancy on DCPM

Appendix C

Source Codes and Relevant Files

Some source codes relevant to this project can be found at https://github.com/ditaanggra29/BESSreliabilityAndCostAnalysis.git.

TRITA-EECS-EX- 2023:527